Theory of hyperfine and superfine levels in symmetric polyatomic molecules. Trigonal and tetrahedral molecules: Elementary spin-1/2 cases in vibronic ground states

William G. Harter*
Joint Institute for Laboratory Astrophysics, National Bureau of Standards and University of Colorado, Boulder, Colorado 80309

Chris W. Patterson
University of California, Los Alamos Scientific Laboratory, Theoretical Division, Los Alamos, New Mexico 87545
(Received 10 August 1978)

A simple approximate scheme for treating molecular hyperfine structure is developed by taking account of energy-level clusters. Unitary tableau and frame transformation techniques are reintroduced. Model Hamiltonians for XY_3 and XY_4 (X spin-zero, Y spin-1/2) molecules are developed and solved in cluster bases which are appropriate for highly excited rotational states. Two cases emerge: Case (1) for which hyperfine splittings are smaller than the "superfine" cluster splittings and case (2) for which superfine splittings are negligible or zero. The problem of correlating energy levels and states between cases (1) and (2) is solved. Since the XY_4 problem in the elementary cluster bases reduces to (2×2) matrices at the worst, the physical interpretation of solutions is not difficult.

I. INTRODUCTION

Modern high-resolution laser spectroscopy has opened up possibilities for understanding molecular structure and dynamics in greater detail than was possible before. High-resolution spectra of heavy symmetric molecules such as SF_6,[1] CF_4,[2] SiF_4, etc., have stimulated the development of a new quantum theory,[3-5] of rotational and vibrational motion for the predominant cases of high angular momentum J. (In heavy molecules the states most easily observed can have J ranging from about 10 or 15 to over 100.) In this theory the properties of energy level and spectral clusters are exploited in order to simplify analysis and calculations involving molecular Hamiltonians. One result of cluster theory is a novel picture of the rotational behavior of spherical top molecules in which the rotational momentum vector becomes "stuck" for awhile on a single internal symmetry axis, and then "tunnels" more or less slowly toward adjacent equivalent axes.

Examples of CF_4 spectra are displayed in Fig. 1 starting with lower resolution and greater frequency scan at the top of the figure. Successively lower stages [(a)–(e)] of Fig. 1 show finer detail seen at higher and higher resolution. The spectral clusters or centrifugal fine structure are clearly visible at stage (c) in the laser diode scan of $P(54)$ by McDowell *et al.*[2] The splitting of clusters due to the angular momentum tunneling or molecular "tumbling" is shown at stage (d) in Fig. 1, and this is called "superfine" structure. Superfine structure has been seen in saturation absorption spectra of SiF_4,[6] CH_4,[7] as well as SF_6,[8,9] and takes very predictable forms. For example, consider the cluster A_1F_1E marked "48" in Fig. 1(c). [The number ($n=48$) is the approximate cluster momentum about the fourfold symmetry axes.] Since there are six fourfold axes the rotational degeneracy of the cluster is six: 1 (for A_1) + 2 (for E) + 3 (for F_1), as first explained by Dorney and Watson[10] who observed clusters in computer experiments. However, a simple tunneling model[3] predicts a splitting of triplet A_1, E, and F_1 into relative energies $-4S{:}0{:}2S$, where S is the tunneling amplitude between adjacent fourfold symmetry axes. The (A_1F_1E) cluster appears again toward the center of $P(54)$ in Figs. 1(c)–1(d) at $n=44$, and again toward the edge at $n=52$, i.e., at all momentum values that equal zero-modulo-four. ($n=0\text{mod}4$.) Other clusters belong to other fourfold axial momenta and to the threefold momentum values on the right-hand side of $P(54)$ in Figs. 1(c)–1(d).[3]

For each type of cluster the tunneling amplitude and corresponding superfine splitting decreases nearly exponentially with the increasing axial momentum number n. These splittings can be derived using approximate formulas[4,11] or else (for $J\leq 100$) obtained from Krohn's computer diagonalizations.[12] For example the A_1F_1E splittings in $P(54)$ are several-hundred megahertz for $n=44$, 2.6 MHz for $n=48$, and 9.4×10^{-6} MHz for $n=52$. Superfine tunneling amplitudes can easily vary over 12 or 15 orders of magnitude within a single $P(J+1)$, $Q(J)$, or $R(J-1)$ manifold for higher values of total angular momentum J.

In this article the interaction between superfine tumbling and nuclear hyperfine spin effects will be discussed. Until recently the nuclear hyperfine interactions have been thought to play a minor role in the rotational behavior of large molecules. The hyperfine splittings themselves are generally

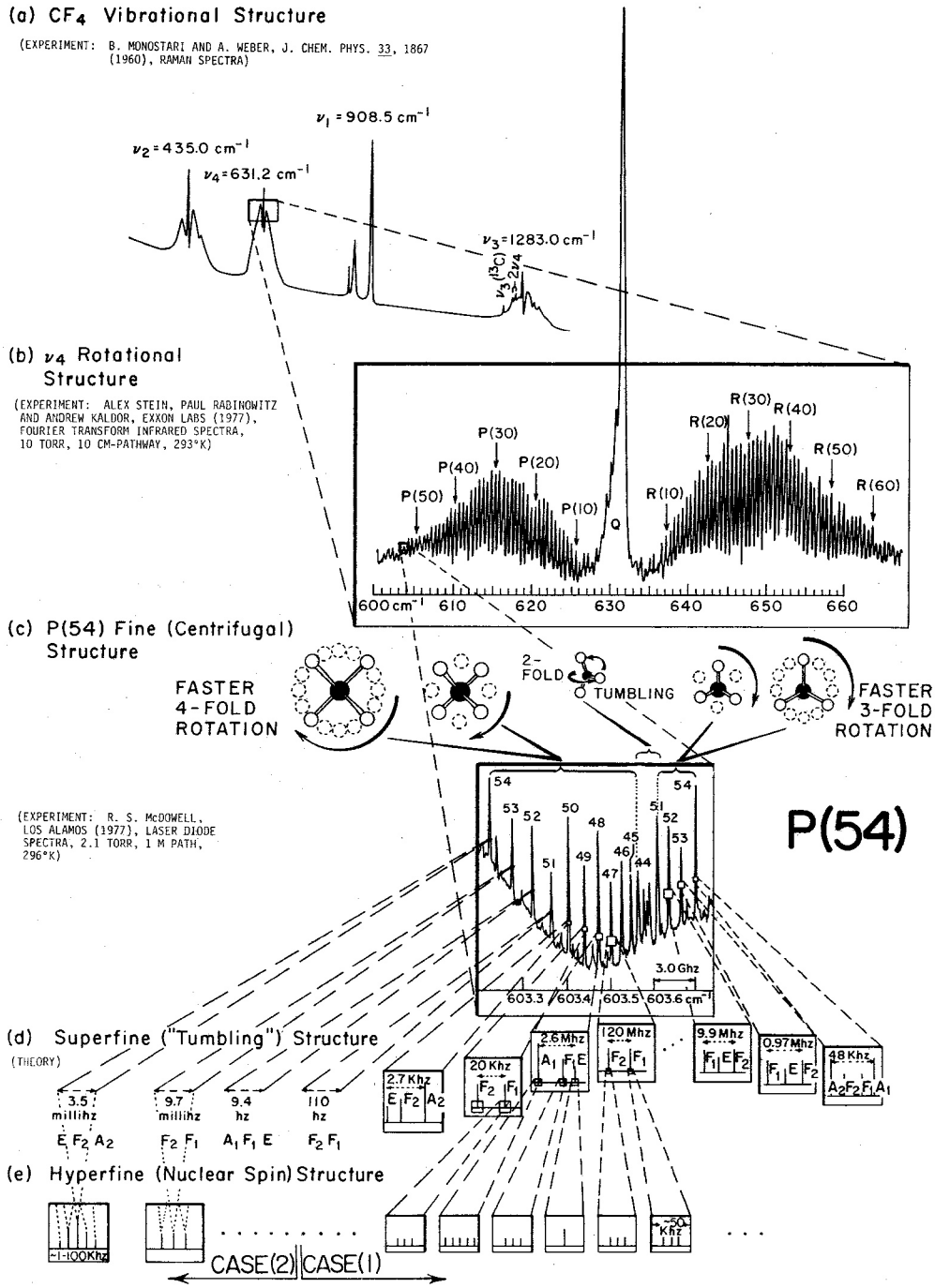

FIG. 1. Spectra of tetraflouromethane (CF_4) [reprinted from *Dimensions*, 62/6 (1978)]. (a) CF_4 vibrational structure [by B. Monostori and A. Weber, J. Chem. Phys. 33, 1867 (1960)] from Raman spectra; (b) ν_4 rotational structure [by Alex Stein, Paul Rabinowitz, and Andrew Kalder, Exxon Labs (1977)] from Fourier transform spectra; 1.3 kPa, 10 cm path, 293 °K; (c) $P(54)$ fine (centrifugal) structure (by R. S. McDowell, H. W. Galbraith, M. J. Reisfeld, and J. P. Aldridge, see also Ref. 2) from laser diode spectra; 280 Pa, 1 m path, 296 °K; (d) superfine ("tumbling") structure. The form of the cluster splitting is predicted by the quantum theory of clusters, but has not yet been observed in CF_4. However, the same structure has been seen in SiF_4, CH_4, and SF_6; (e) hyperfine ("nuclear spin") structure. The hyperfine structure falls into two cases: a "normal" case (1) in which the spin multiplets are well separated, and case (2) where they overlap and may interact.

a few kilohertz and could be seen only in the large saturation absorption chambers used by Hall and Borde[13] to study CH_4 and by Borde and Borde[14] to study SF_6. However, it may not take much of a nuclear-spin-rotation interaction to affect a CF_4 molecule which is in a cluster state having *millihertz* superfine splittings! Even if no spin interactions existed at all, a CF_4 molecule set spinning on one body axis could, depending on which quantum states were chosen, easily stay on that axis for seconds, minutes, or even years before tumbling. Hence, even for the smallest hyperfine interactions there will always be superfine cluster states with which the spin states can interact resonantly. Roughly speaking the spins can align themselves with the body symmetry axis used by the cluster state, and while acting like miniature gyroscopes, they can further stabilize the molecule against tumbling.[15]

Once a molecule becomes spin stabilized, the spin-permutation states belonging to species labels $A_{1,2}$, E, or $F_{1,2}$ may be mixed. This can happen because certain identical nuclei which normally permute freely amongst themselves, become segregated once tumbling is quenched. To recover a meaningful internal symmetry label of nuclear permutational properties one must appeal to the algebra of the spontaneously broken symmetry. This requires an understanding of the effects of combined centrifugal distortion and nuclear-spin-rotation Hamiltonians as one effect becomes stronger or weaker than the other.

The following sections will be devoted to obtaining simple approximate eigensolutions of centrifugal and nuclear-spin-rotation Hamiltonians, with an emphasis on the physical understanding of the results. We use three different theoretical methods which have recently seen considerable development but have heretofore remained largely disconnected. The three areas, starting with the most recently developed, are (i) the quantum theory of level clusters, (ii) the theory of frame transformation relations, and (iii) the theory of Weyl or Young tableau labeling of permutation and unitary states of several identical fermions or bosons. The methods of level cluster theory are described in Refs. 3–5, and applied to spectral analysis in Ref. 16. The methods of frame transformation theory are introduced and applied by Fano and by Chang and Fano[17] to diatomic and symmetric top molecules, and generalized to polyatomic molecules in Ref. 5. The methods of permutation-group tableau labeling were introduced by Young and Rutherford,[18] Weyl,[19] and later by Goddard[20] for treating molecular electronic orbitals. The development of unitary tableaus as a calculus for matrix elements is treated in Refs. 21–24, and is based upon mathematical works of Weyl,[19] Gelfand,[25] Biedenharn,[26] and Louck.[27] The application of tableaus to molecular spin state and statistical weight calculations is introduced in Ref. 5. (A similar treatment which does not emphasize tableau calculus is given by Galbraith.[28])

The present work complements previous treatments of polyatomic molecular hyperfine structure.[29,30] It simplifies the analysis of states involving large angular momentum which would otherwise seem to require tedious numerical computation. Certain of our simplifications resemble those used by Levenson and Schawlow[31] to treat rapidly rotating diatomic molecules. However, our principle aim is to develop a polyatomic symmetry labeling scheme that is a useful generalization of the diatomic "ortho" and "para" labeling. This is particularly important in our case (2) where centrifugal superfine and nuclear hyperfine effects can combine to mix the standard rovibrational species labels. So far, standard symmetry labeling has been used by Quack[32] to derive selection rules for chemically reactive scattering, but no account of clustering or hyperfine structure has been taken. Now we can begin to remedy this situation with the help of this work and modern laser spectroscopy.

II. THEORY OF ROTATIONAL CLUSTER AND NUCLEAR-SPIN STATES: AN XY_3 EXAMPLE

A. Orbital states and permutational symmetry

It is convenient to start with a basis of rotational "cluster" states $|{}^{N^p}_{mn}\rangle$ which have total nuclear angular momentum parity N^p (N is labeled R for "rotor" in many other works), laboratory-fixed azimuthal momentum m, and body-fixed momentum component n, projected upon a certain internal axis (n is labeled K_R in many other works) preselected according to arguments of cluster theory. Each state $|{}^{N^p}_{mn}\rangle$ is a combination of states $R(\alpha\beta\gamma)|1\rangle$ and $I\cdot R(\alpha\beta\gamma)|1\rangle$ of definite rotational position described by Euler angles $(\alpha\beta\gamma)$ and the absence or presence of inversion (I) from an "original" state $|1\rangle$ in which body axes $(\overline{xyz})$ coincide with lab axes (xyz). As explained in other works[5] these states are obtained by applying orthogonal group (O_3) projection operators ($P^{N^p}_{mn}$) to the original state $|1\rangle$, i.e., let

$$|{}^{N^p}_{mn}1\rangle = P^{N^p}_{mn}|1\rangle/\sqrt{[N]} = \sum\int d(\alpha\beta\gamma)\mathfrak{D}^{N^p}_{mn}{}^{*}[O(\alpha\beta\gamma)]O(\alpha\beta\gamma)|1\rangle\sqrt{[N]}, \tag{2.1}$$

where $\mathfrak{D}^{N}_{mn}$ are the irreducible representations of O_3 and the integral sum is over all proper ortho-

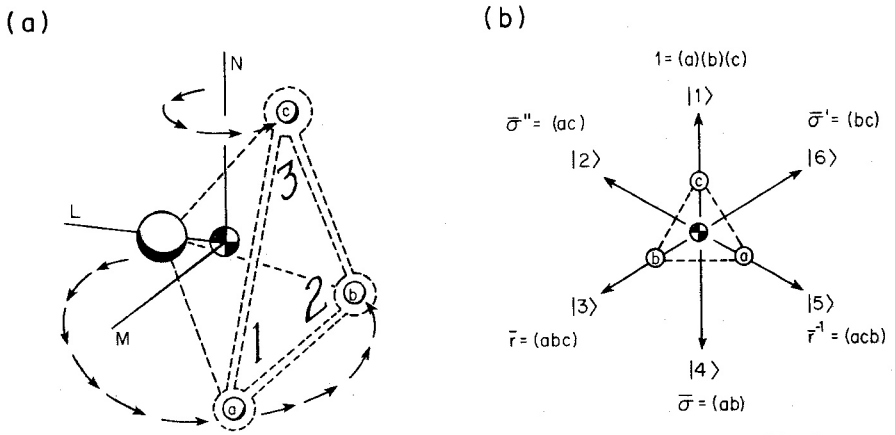

FIG. 2. XY_3 molecule in twofold axial rotational states. (a) The Y particles are labeled by letters a, b, and c, while the states in which they may reside are numbered 1, 2, or 3. The states are distinguishable while the particles are indistinguishable, and a given particle can reside just as well in any of the three states. State 3 is always closest to the rotation axis. (b) Each permutation of particles between the states corresponds to a different direction for the twofold rotation axis (N) *with respect to the particles*, a, b, and c. For each direction one defines a cluster base state $|1\rangle$, $|2\rangle$, ..., $|6\rangle$.

gonal operators $O(\alpha\beta\gamma)=R(\alpha\beta\gamma)$, i.e., all rotations, as well as all improper operators $O(\alpha\beta\gamma)=I\cdot R(\alpha\beta\gamma)=R(\alpha\beta\gamma)\cdot I$, i.e., all rotation inversions. The resulting states have definite parity, i.e.,

$$I|^{N^{\pm}}_{mn}1\rangle=\pm|^{N^{\pm}}_{mn}1\rangle \tag{2.2}$$

as well as simple rotational properties

$$\bar{R}(\alpha OO)|^{N^{\pm}}_{mn}1\rangle=e^{\alpha n/i}|^{N^{\pm}}_{mn}1\rangle \tag{2.3}$$

with respect to *internal* rotations around the preselected $\bar{z}$ body axis.

States of rotation around a single internal body axis ($\bar{z}$) are only approximate eigenstates if there is any cluster splitting. Better approximations are obtained by considering linear combinations of states

$$\{|^{N^p}_{mn}1\rangle,\ |^{N^p}_{mn}\bar{r}\rangle=\bar{r}|^{N^p}_{mn}1\rangle,\ |^{N^p}_{mn}\bar{r}'\rangle=\bar{r}'|^{N^p}_{mn}1\rangle,\ldots\}$$

of rotation about all symmetry axes equivalent to the primary $\bar{z}$ axis. The proper combinations may be obtained by applying internal symmetry projectors $P^{\{\mu\}}_{\{i\}\{j\}}$ to the primary state $|^{N^p}_{mn}1\rangle$, i.e., let

$$|^{N^p\{\mu\}}_{mn\{i\}\{j\}}\rangle=P^{\{\mu\}}_{\{i\}\{j\}}|^{N^p}_{mn}1\rangle/\sqrt{\mathfrak{N}}$$

$$=\sum_{\bar{r}}\mathfrak{D}^{\{\mu\}*}_{\{i\}\{j\}}(\bar{r})\bar{r}|^{N^p}_{mn}1\rangle(l^{\{\mu\}}/{}^{\circ}g\sqrt{\mathfrak{N}}\,, \tag{2.4}$$

where $\bar{r}$ are internal symmetry operations which have the effect of changing the internal rotation axis, $\mathfrak{D}^{\{\mu\}}_{ij}$ are irreducible representations of an appropriate finite internal symmetry group $\bar{g}$ of order ${}^{\circ}g$, $l^{\{\mu\}}$ is the dimension of $\mathfrak{D}^{\{\mu\}}$, and $\mathfrak{N}$ is the norm. Note that internal operations always commute with external ones ($\bar{r}R=R\bar{r}$).

It is convenient to relate finite internal symmetry operations ($\bar{r}$) with permutations, and then associate the representation labels $\{\mu\}$ and $\{i\}$ or $\{j\}$ with arrangements of boxes called Young frames and tableaus, respectively. This box notation is one of the most powerful notational schemes that has been developed for quantum physics, and we shall attempt to show some of its uses by examples.

As a simple example consider a C_{3v} symmetric ammonialike molecule XY_3 as shown in Fig. 2. Here it is assumed that twofold axes point along centrifugal distortion extrema that are of sufficient depth to "capture" the angular momentum vector. It is not yet known what the conditions must be in order to have twofold clusters[3,5] in spectra of symmetric top molecules. However, there must exist a least upper bound for the N quantum number beyond which twofold rotation and related spectral clustering is present; this is well-known behavior of a classical semirigid C_{3v} rotor. [For a prolate ($I_A=I_B>I_C$) top twofold rotational states would actually be lowest in energy.] Nevertheless, the XY_3 example is a good tutorial device for explaining the use of cluster theory in more complicated heavy spherical top molecules where the clusters have shown up in every spectrum of sufficient resolution taken so far.

There are six states

$$\{|^{N^p}_{mn}1\rangle,\ |^{N^p}_{mn}\bar{r}\rangle,\ |^{N^p}_{mn}\bar{r}^{-1}\rangle|^{N'}_{mn}\bar{\sigma}\rangle|^{N^p}_{mn}\bar{\sigma}'\rangle,\ |^{N^p}_{mn}\bar{\sigma}''\rangle\}$$

for each value of momenta N^p, m, and n. These correspond to each of six equivalent twofold axes along which the momentum vector N could "stick," as indicated by arrows in Fig. 2(b). Note that each of these states may be obtained from the original state $|^{N}_{mn}1\rangle$ by a permutation of the Y_3 nu-

clei a, b, or c in Fig. 2(a). For example, the permutation (abc) moves (a) to where (b) was, (b) to where (c) was, and (c) back to where (a) was. In the original state $|{}^{N\rho}_{mn}1\rangle$ nuclei (a) and (b) occupy the "wing" states numbered 1 and 2, respectively, in Fig. 2(a) where they sit away from the angular momentum axis and hence they move faster than nucleus (c) which sits in "apex" state 3 practically on top of the N axis. However, in state $|{}^{N\rho}_{mn}\bar{r}\rangle$ obtained by permutation (abc) we find that nucleus (b) winds up in the apex state 3 [see Figs. 2(a) and 2(b)]. Operation $\bar{r}=(abc)$ can be thought of as a 120° internal rotation around the C_{3v} threefold axis of the XY_3 molecule. Operations such as $\sigma=(ab)$ are planar reflections, i.e., 180° rotation inversions.

One should not confuse the LMN frame in Fig. 2(a) with an Eckart frame.[33] The N axis always stands for the axis of quantization for all the approximate cluster bases regardless of which nuclei reside in "pockets" or states 1, 2, or 3. The states are distinguished by different physical properties (viz., states 1 and 2 give nuclei faster rides than state 3) while nuclei are apart from their spins quite identical. Hence the nuclear labels a, b, and c must finally be summed to give a physically meaningful quantum state. This is indeed what happens when the Pauli principle is invoked as we will see in Sec. IIB.

The representations $\mathfrak{D}^{\{\mu\}}_{ij}$ of permutation group S_3 are labeled by Young frames of three boxes in a row $\{3\}$, three boxes in a column $\{111\}$, and an arrangement $\{2,1\}$ with two boxes in the first row and one in the second. Normally, the representations $\{3\}$, $\{111\}$, and $\{2,1\}$ would be called A_1, A_2, and E, respectively, or else A', A'', and E or any of the many notations that exist in the literature. The Young frames and tableaus present the opportunity to eliminate once and for all the confusion and vagueness of proliferating group-theoretical and molecular-symmetry notations. Furthermore, the tableaus become nomograms or mnemonics for producing "on demand" the entries to all sorts of character, representation, and transformation tables that normally must be stored in the back of textbooks; hence tableaus minimize the chances for errors of typography or mischosen phases. As an example the representations $\mathfrak{D}^{\{3\}}$, $\mathfrak{D}^{\{111\}}$, and $\mathfrak{D}^{\{2,1\}}$ are derived in Appendix A. The results are used in Eq. (2.4) to give in Fig. 3 the "angular-momentum-tunneling" wave states of a trigonal molecule. It is as important to make a distinction between the left $\{i\}$ and right $\{j\}$ subindices of the projector $P^{\{\mu\}}_{ij}$ in Eq. (2.4) as it is to distinguish m and n in the O_3 projector $P^{N\rho}_{mn}$ [Eq. (2.1)]. To emphasize the difference we generally replace the *particle* labels a, b, and c in the right-hand $\{j\}$ tableau by the *state* labels of the state in which *each particle resides in the original state*, i.e., $a\to 1$, $b\to 2$ and $c\to 3$. The right-hand $\{j\}$ tableaus determine the physically distinct (state) properties of the wave function, while the left-hand $\{i\}$ tableaus merely determine the properties of the wave function *vis-à-vis* permutation of particles a, b, and c.[34] In the language of Refs. 23 and 34 (in the latter the order is reversed), the left-hand indices (i) label permutational group S_n bases while the right-hand indices (j) label unitary group U_m bases. The general problem treated there is that of n indistinguishable particles occupying m distinguishable states. Here we happen to have $n=3$ particles to occupy the same number $(m=3)$ of states, and we do not consider the possibility of more than one particle at a time occupying a given state.

As we will see the left-hand indices

$$\{i\}=\begin{array}{|c|c|}\hline a & b\\\hline c\\\cline{1-1}\end{array}\quad\text{and}\quad\begin{array}{|c|c|}\hline a & c\\\hline b\\\cline{1-1}\end{array}$$

will be summed in a particular way to satisfy the Pauli exclusion principle. Hence this twofold "i degeneracy" is fictitious. However, the "j degeneracy" associated with right-hand indices

$$\{j\}=\begin{array}{|c|c|}\hline 1 & 2\\\hline 3\\\cline{1-1}\end{array}\quad\text{and}\quad\begin{array}{|c|c|}\hline 1 & 3\\\hline 2\\\cline{1-1}\end{array}$$

is quite real; it corresponds to inversion doublet states. To see this note that the point group C_{3v} has three improper planar reflection operations $\bar{\sigma}$, $\bar{\sigma}'$, and $\bar{\sigma}''$ which correspond to the three odd elementary transposition permutations (ab), (bc), and (ac), respectively. A plane reflection such as $\bar{\sigma}=(ab)$ is a product of inversion (I) with a 180° rotation about the normal axis. In case of $\bar{\sigma}$ the rotation is $\bar{R}(0\,180°\,0)$ about the $\bar{y}$ or M axis in Fig. 2 hence

$$(ab)=\bar{\sigma}=\bar{I}\bar{R}(0\,180°\,0)=\bar{R}(0\,180°\,0)\bar{I}\,.$$

The effect of $\bar{\sigma}$ on the original state $|{}^{N\rho}_{mn}1\rangle$ is the following

$$\begin{aligned}\bar{\sigma}|{}^{N\rho}_{mn}1\rangle&=\bar{R}(0\,180°\,0)\bar{I}\,|{}^{N\rho}_{mn}1\rangle\\&=\bar{R}(0\,180°\,0)(-1)^{\rho}|{}^{N\rho}_{mn}1\rangle\\&=(-1)^{\phi(n)}(-1)^{\rho}|{}^{N\rho}_{m-n}1\rangle\,,\end{aligned}\tag{2.5a}$$

where the phase $\phi(n)$ depends upon the choice of convention for $\mathfrak{D}$ matrices in Eq. (2.1). Our choice gives

$$\phi(n)=N-n\,.\tag{2.5b}$$

However, regardless of the choice for $\phi(n)$ there are two types of wave states; one for each choice of parity p, and different choices can in general give states of different energy.

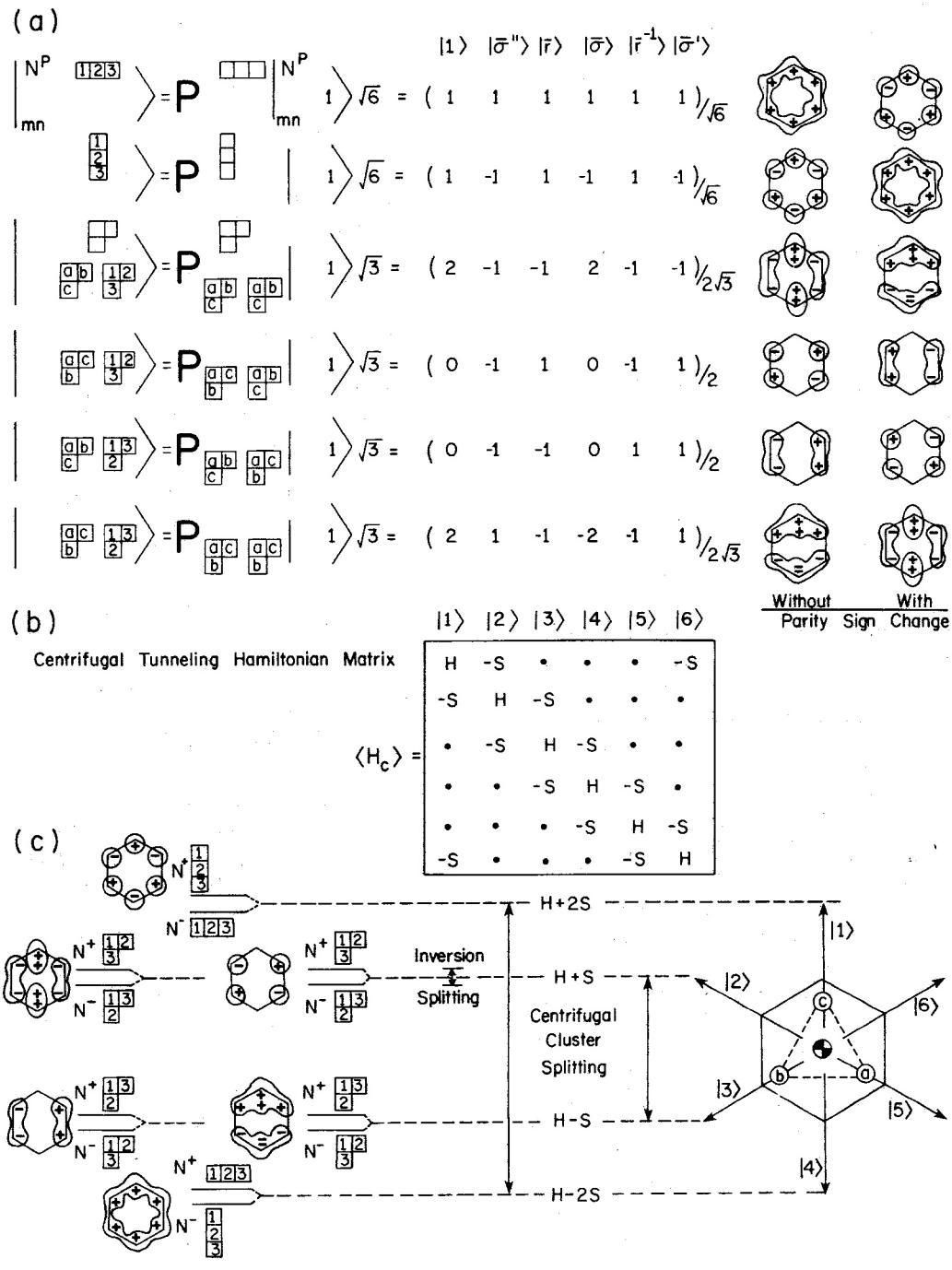

FIG. 3. Twofold cluster eigenstates and energy levels for XY_3 molecule. (a) Tableau projectors give eigenstates according to (2.4), and the angular momentum "wave picture" of the states depends on the parity according to (2.5a); (b) Centrifugal tunneling matrix assumes a tunneling amplitude(s) between nearest-neighbor axes only. H is the "center of gravity" of the cluster; (c) cluster level structure results from matrix (b) and eigenvectors (a).

To determine the energy levels in the cluster approximation we construct an angular-momentum-tunneling matrix in Fig. 3(b) by assuming nonzero tunneling amplitudes ($-S$) to exist only between adjacent axes, i.e., only between axes 1 and 2, 2 and 3, 3 and 4, etc, in Fig. 2(b). Let cluster states $|1\rangle$ and $|4\rangle$ be

$$|1\rangle = |{}^{N\hat{P}}_{mn}1\rangle, \quad |4\rangle = \bar{R}(0\,180°0)|{}^{N\hat{P}}_{mn}1\rangle = (-1)^{\phi(n)}|{}^{N\hat{P}}_{m-n}1\rangle \tag{2.6a}$$

whereupon all six cluster states are obtained by rotations of the original state $|1\rangle$

$$|2\rangle=\bar{r}^{-1}|4\rangle,\quad |3\rangle=\bar{r}|1\rangle,$$
$$|5\rangle=\bar{r}^{-1}|1\rangle,\quad |6\rangle=\bar{r}|4\rangle. \tag{2.6b}$$

The bases $\{|1\rangle,|2\rangle,|3\rangle,\ldots,|6\rangle\}$ differ at most by phases from bases $\{|1\rangle,|\bar{\sigma}''\rangle,|r\rangle,\ldots,|\bar{\sigma}'\rangle\}$, but they are more convenient when improper reflections or inversion rotations are physically less feasible than rotations. Then the rotational cluster splitting $\pm S$ and $\pm 2S$ dominates the inversion splitting $H^{\pm}$ between doublet states of different parity as shown in Fig. 3(c). The energy levels shown there are obtained by substituting the eigenvectors in Fig. 3(a) into a Schrödinger equation

$$H|{}^{N\mathcal{P}(\mu)}_{n\ \{j\}}\rangle=e|{}^{N\mathcal{P}(\mu)}_{n\ \{j\}}\rangle \tag{2.7}$$

involving the Hamiltonian matrix in Fig. 3(b).

B. Spin states and the Pauli principle

The general three-particle spin state will be denoted by $|s,s',s''\rangle$ which means nucleus a is in state s, b in s', and c in s''. For spin-$\frac{1}{2}$ nuclei, two base states "up" ($\uparrow$) and "down" ($\downarrow$) exist for each nucleus, and so there are $2^3=8$ spin base states for the XY_3 molecule if nucleus X has no spin.

The tableau projection operators $P^{\{\mu\}}_{\{i\}\{j\}}$ can be used to produce definite total nuclear-spin I states

$$|{}^{\{\mu\}}_{\{i\}\{k\}}\ {}^{I}_{m_I}\rangle=P^{\{\mu\}}_{\{i\}\{k\}}|s,s',s''\rangle/(\mathfrak{N}), \tag{2.8}$$

where the original spin states $|s,s',s''\rangle$ are just those for which $s\geq s'\geq s''$, i.e., $|\uparrow,\uparrow,\uparrow\rangle$, $|\uparrow,\uparrow,\downarrow\rangle$, $|\uparrow,\downarrow,\downarrow\rangle$, or $|\downarrow,\downarrow,\downarrow\rangle$. Applying the projection operators in Appendix A to these states gives the eight states shown in Fig. 4. It is shown in Refs. 20–23 that tableaus $\{3\}$ and $\{2,1\}$ correspond to total spin $I=\frac{3}{2}$ and $\frac{1}{2}$, respectively, while the tableau $\{1,1,1\}$ fails to produce any states since totally antisymmetric combinations of three spin-$\frac{1}{2}$ states must vanish. (In general, two-rowed tableaus $\{\mu_1,\mu_2\}$ give spin $I=\frac{1}{2}(\mu_1-\mu_2)$ combinations of $n=\mu_1+\mu_2$ spin-$\frac{1}{2}$ particles while three-or-more-rowed tableaus contribute nothing.) The right-hand tableau index $\{k\}$ of the $\{2,1\}$ projector has the a, b, and c labels replaced by the labels of the states in which the respective particles are

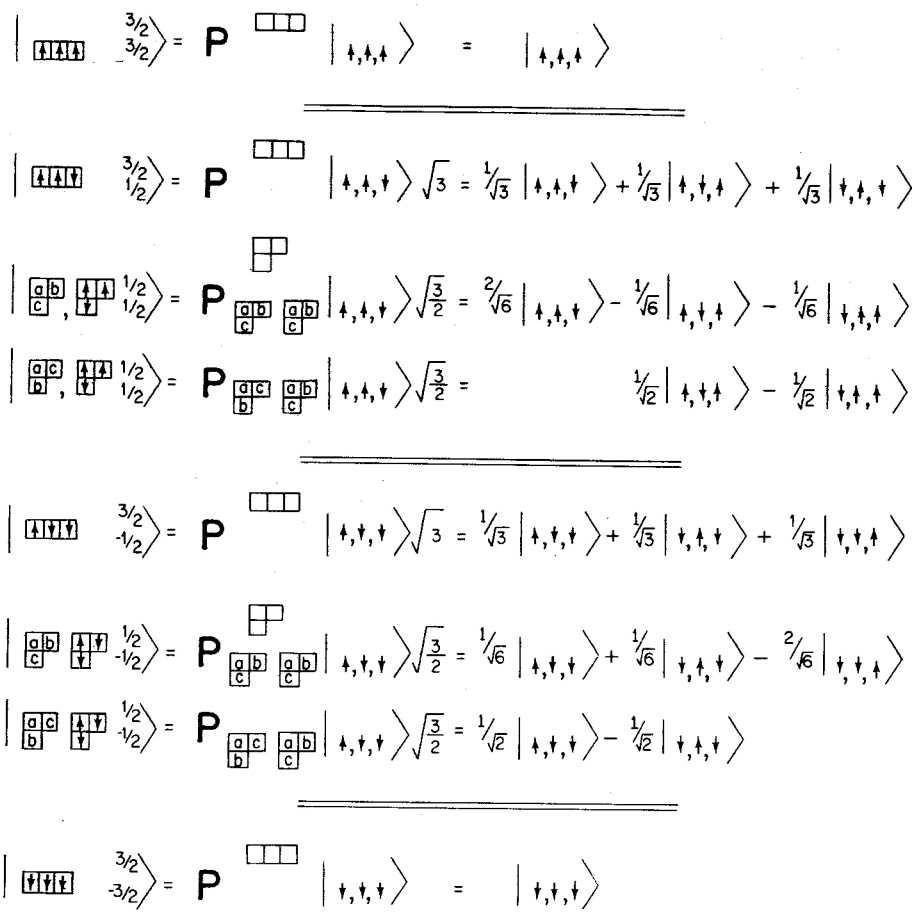

FIG. 4. XY_3 spin states. States are labeled both by tableaus and the standard $|{}^{I}_{m_I}\rangle$ angular momentum numbers.

residing in the original state. For example,

$$\{k\}=\begin{array}{|c|c|}\hline a & b\\\hline c\\\cline{1-1}\end{array}$$

acting on $\{\uparrow,\downarrow,\downarrow\rangle$ is rewritten $\{k\}=\begin{smallmatrix}\uparrow\\\downarrow\uparrow\end{smallmatrix}$. This notation by itself will be sufficient to define the physical properties of the state in Eq. (2.8); we can just as well drop the $I=\frac{1}{2}$, $m_I=-\frac{1}{2}$, and the left-hand $\{i\}$ tableau index will be summed shortly to satisfy the Pauli principle. Had we chosen the other possibility

$$\{k\}=\begin{array}{|c|c|}\hline a & c\\\hline b\\\cline{1-1}\end{array}$$

for the right-hand index of the projector $P^{\{2,1\}}_{\{i\}\{k\}}$ no new states would arise from action on $\{\uparrow,\downarrow,\downarrow\rangle$, and action on $|\uparrow,\uparrow,\downarrow\rangle$ gives *zero*. (Indeed, $\{k\}=\begin{smallmatrix}\uparrow\uparrow\\\downarrow\end{smallmatrix}$ is a null tableau; equal states cannot reside together in a tableau column since columns stand for antisymmetrization.)

Finally, Pauli antisymmetric states, which are the only ones allowed for spin-$\frac{1}{2}$ Fermi particles, are obtained from particular combinations of the orbital states in Eq. (2.4) and the spin states in Eq. (2.8). For each tableau $\{i\}$ there is a *conjugate* one denoted by $\{\tilde{i}\}$ in which rows and columns are switched. For example, we would have

$$\begin{array}{|c|c|}\hline 1 & 2\\\hline 3\\\cline{1-1}\end{array}=\begin{array}{|c|c|}\hline 1 & 3\\\hline 2\\\cline{1-1}\end{array},\qquad \begin{array}{|c|c|}\hline 1 & 2\\\hline 3\\\cline{1-1}4\\\cline{1-1}\end{array}=\begin{array}{|c|c|c|}\hline 1 & 3 & 4\\\hline 2\\\cline{1-1}\end{array},\quad \text{or } \{\tilde{3}\}=\{1,1,1\}.$$

Pauli antisymmetric states are made of products of states belonging to $\{\mu\}$ and $\{\tilde{\mu}\}$ orbit and spin tableaus, respectively, as follows:

$$|{}^{N^p}_{mn}\{j\}\{\tilde{k}\}^I_{m_I}\rangle=\sum_{\{i\}}\frac{(-1)^{p_i}}{(l^\mu)^{1/2}}\,|{}^{N^p\{\mu\}}_{mn\{i\}\{j\}}\rangle\,|{}^{\{\tilde{\mu}\}}_{\{\tilde{i}\}\{\tilde{k}\}}{}^{I}_{m_I}\rangle\,, \tag{2.9a}$$

where l^μ is the dimension[35] of $S_n=S_3 IR\{\mu\}$,

$$l^\mu=n!/(\text{product of }\{\mu\}\text{ hook lengths}), \tag{2.9b}$$

and p_i is the parity [(+) for even and (−) for odd] of the permutation that converts tableau $\{i\}$ into the "first" one $\{i_1\}$ wherein the particle labels a, b, c, are lexocographically inserted in frame $\{\mu\}$.

Some examples will be given now. The $\{\mu\}=\{1,1,1\}$ state

$$\left|{}^{N^p}_{mn}\begin{array}{|c|}\hline 1\\\hline 2\\\hline 3\\\cline{1-1}\end{array}\ \uparrow\uparrow\uparrow\ {}^{3/2}_{3/2}\right\rangle=\left|{}^{N^p}_{mn}\begin{array}{|c|}\hline 1\\\hline 2\\\hline 3\\\cline{1-1}\end{array}\right\rangle\left|\uparrow\uparrow\uparrow\ {}^{3/2}_{3/2}\right\rangle \tag{2.10}$$

requires no sum and obviously satisfies the Pauli principle. The $\{\mu\}=\{2,1\}$ state

$$\left|{}^{N^p}_{mn}\begin{array}{|c|c|}\hline 1 & 2\\\hline 3\\\cline{1-1}\end{array}\ {}^{\uparrow\uparrow\ 1/2}_{\downarrow\ \ 1/2}\right\rangle=\frac{1}{\sqrt{2}}\left(\left|{}^{N^p\{2,1\}}_{mn}\begin{array}{|c|c|}\hline a & b\\\hline c\\\cline{1-1}\end{array}\begin{array}{|c|c|}\hline 1 & 2\\\hline 3\\\cline{1-1}\end{array}\right\rangle\left|\begin{array}{|c|c|}\hline a & c\\\hline b\\\cline{1-1}\end{array}\ {}^{\{2,1\}\ \ 1/2}_{\uparrow\uparrow\ \ 1/2}\right\rangle-\left|{}^{N^p\{2,1\}}_{mn}\begin{array}{|c|c|}\hline a & c\\\hline b\\\cline{1-1}\end{array}\begin{array}{|c|c|}\hline 1 & 2\\\hline 3\\\cline{1-1}\end{array}\right\rangle\left|\begin{array}{|c|c|}\hline a & b\\\hline c\\\cline{1-1}\end{array}\ {}^{\{2,1\}\ \ 1/2}_{\uparrow\uparrow\ \ 1/2}\right\rangle\right) \tag{2.11}$$

is more complicated but can be shown to be Pauli antisymmetric as well.

There is a convenient tableau formula[22,23] for relating orbit-spin states such as (2.9), (2.10), or (2.11) to Slater determinant states. Examples of Slater states are

$$\left|{}^{N^p}_{mn}\ {}^{1\uparrow}_{2\uparrow}_{3\uparrow}\right\rangle$$

or

$$\left|{}^{N^p}_{mn}\ {}^{1\uparrow}_{2\downarrow}_{3\uparrow}\right\rangle,$$

$1\uparrow$

etc. The notation $2\downarrow$, for example, stands for

$3\uparrow$

the completely antisymmetric sum

$$\left|{}^{N^p}_{mn}\ {}^{1\uparrow}_{2\downarrow}_{3\uparrow}\right\rangle=\sum_r\frac{(-1)^{P_r}}{\sqrt{3!}}\left\{(r)_{\text{orbit}}\left|{}^{N^p}_{mn}\,1\right\rangle\right\}$$
$$\times\{(r)_{\text{spin}}|\uparrow,\downarrow,\uparrow\rangle\} \tag{2.12}$$

over all permutations (r) of nuclei a, b, and c such that any nuclei in states 1 and 3 have spin "up" ($\uparrow$) while any nucleus in state 2 always has spin "down" ($\downarrow$). This Slater determinant state $\left|{}^{1\uparrow}_{2\downarrow}_{3\uparrow}\right\rangle$ would be written $|(1^+)(2^-)(3^+)\rangle$ in the standard notation of electronic orbital theory, however, we prefer to reserve the horizontal format for the Slater "permanent" state which will be needed to describe *Bose* symmetrization of integral-spin nuclei. Figure 5 shows how to relate orbit-spin states to Slater states using the tableau "assembly formula," and an example relevant to the XY_3 problem is worked out. The assembly formula makes it possible to transform between the two types of states [Eqs. (2.9) and (2.12)] without getting involved in any sums over $n!$ permutations. The transformation is useful since Slater-type states are convenient for constructing Hamiltonians while orbit-spin states are convenient for describing eigenvectors.

It is instructive to use Fig. 5 to obtain the trans-

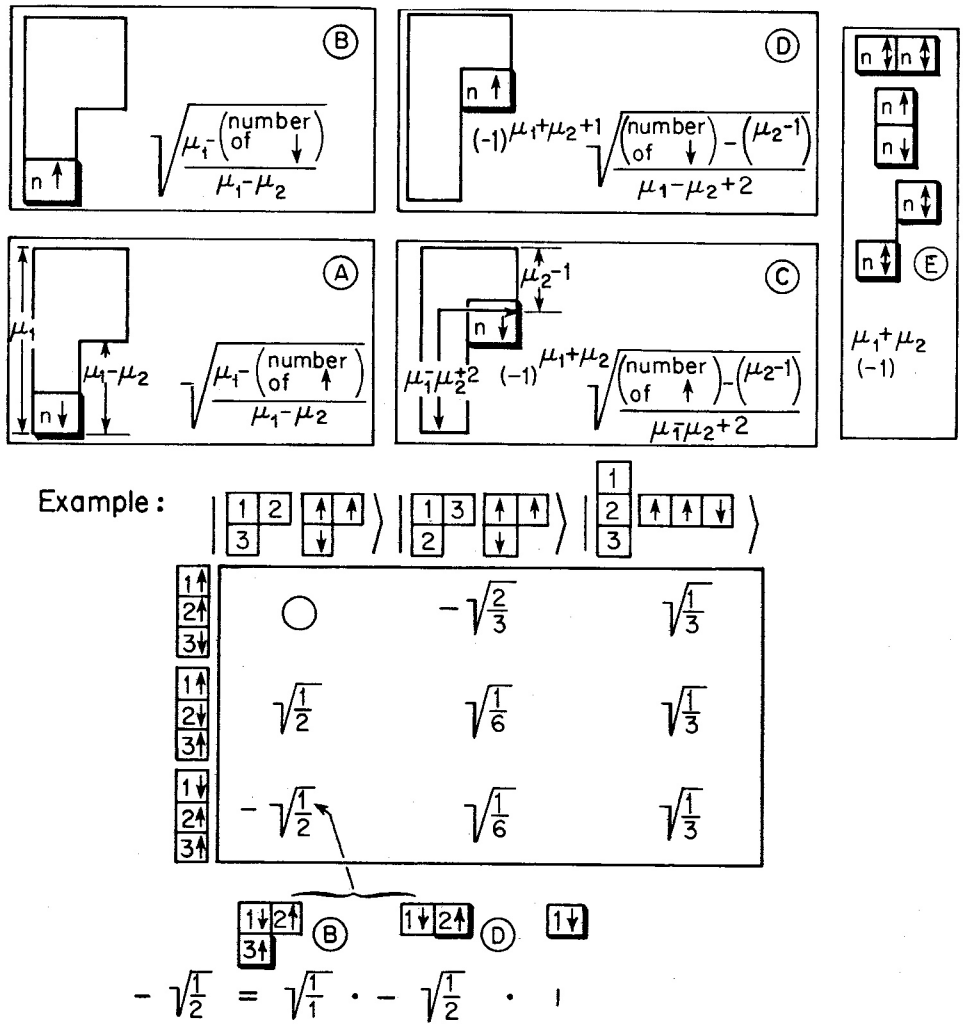

FIG. 5. Assembly formula for combining orbital and spin states. Each column state (Slater determinant) on the left-hand side of the sample table has a definite spin (arrow) on each orbital state (number). The formulas will give the overlap of this Slater state with a given orbital tableau state if one first writes the spin within this orbital tableau in exactly the same way. Then one proceeds to remove boxes with numbered spins starting with the highest number(s). Each "removal" gives a factor depending on what is being removed and where (cases A–E). All of the numbers in the formulas refer to the condition of the tableau just before the box outlined in the figure is removed.

formation

$$T = \begin{array}{c|cc} & \left|\boxed{1\,2}\,{\uparrow\atop\downarrow}\right\rangle\left|\boxed{1\atop 2}\,\uparrow\downarrow\right\rangle \\ \hline 1\uparrow 2\downarrow & 1/\sqrt{2} & 1/\sqrt{2} \\ 1\downarrow 2\uparrow & -1/\sqrt{2} & 1/\sqrt{2} \end{array} \tag{2.13}$$

from Slater states to "para" (singlet) and "ortho" (triplet) states involving just two spin-$\frac{1}{2}$ nuclei.

C. Angular momentum states and spin frame transformations

In the limit of weak spin-rotation coupling the hyperfine eigenstates will be the following combinations:

$$|{}^{N^p}_{n}\{j\}^{F^p}_{f}\rangle = \sum C^{\,I\ N\ F}_{m_I\ m_f\ m}\,|{}^{N^p}_{mn}\{j\}\{\bar{k}\}^{\,I}_{m_I}\rangle \tag{2.14}$$

of the orbit-spin states from Eq. (2.9), where C^{INF} are Clebsch-Gordan coefficients and the total momentum operator is the sum

$$\vec{F} = \vec{N} + \vec{I} \tag{2.15}$$

of nuclear rotor ($\vec{N}$) and nuclear-spin ($\vec{I}$) momentum operators. For these states the N, I, and F quantum numbers are good as are the lab (z) component f of F and the body ($\bar{z}$) component n of N (n is the cluster momentum number). The spin states are assumed to have positive parity. The spin momentum is quantized in the lab (z) axis.

If spin-rotation-induced hyperfine splitting equals or exceeds the centrifugal superfine or cluster splitting then states with the nuclear spins quantized in the body frame become useful bases. These states will be denoted by overlined ($\bar{\uparrow}$, or $\{\bar{k}\}$) spin tableaus as in the following example:

$$|\{j\}\{\bar{\bar{k}}\}^{F^p}_{f,\,\bar{f}=n+\bar{n}_I}\rangle = \left|\boxed{\begin{array}{cc}1&2\\3&\end{array}}\ \begin{array}{l}\bar{\downarrow}\bar{\downarrow}\ F^p\\ \bar{\downarrow}\ \ f,\bar{f}=n-1/2\end{array}\right\rangle, \tag{2.16}$$

where f and $\bar{f}$ are lab and body components, re-

TABLE I. Spin frame relation for angular momentum $I=\frac{1}{2}$.

	$\left\vert \begin{array}{|c|c|}\hline 1&2\\\hline 3\\\cline{1-1}\end{array}\ \bar{\uparrow}\,\uparrow \right\rangle$	$\left\vert \begin{array}{|c|c|}\hline 1&2\\\hline 3\\\cline{1-1}\end{array}\ \bar{\uparrow}\,\downarrow \right\rangle$
$\left\langle N\ \begin{array}{|c|c|}\hline 1&2\\\hline 3\\\cline{1-1}\end{array}\ F=N+1/2 \right\vert$	$\left(\frac{N+n+1}{2N+2}\right)^{1/2}$	$-\left(\frac{N-n+1}{2N+2}\right)^{1/2}$
$\left\langle N\ \begin{array}{|c|c|}\hline 1&2\\\hline 3\\\cline{1-1}\end{array}\ F=N-1/2 \right\vert$	$\left(\frac{N-n}{2N}\right)^{1/2}$	$\left(\frac{N+n}{2N}\right)^{1/2}$

spective of the total momentum F, and n_I is the body component of the total nuclear spin. (n_I can be read directly from the spin tableau $\{\bar{k}\}$.)

Transformations between body spin states [Eq. (2.16)] and lab spin states [Eq. (2.14)] are analogous to the frame transformations between states belonging to different Hunds cases. These have been exploited extensively by Fano and Chang[17] in treatments of molecular electronic orbitals. After the notational changes $l\to I$, $\Lambda\to\bar{n}_I$, $J\to F$, and $K\to\bar{f}$ in Eq. (3.6) of Ref. 5 the following relation results:

$$|{}^{N^p}_{n}\{j\}^{F^p}_{f}\rangle=\sum_{\bar{n}_I}\left(\frac{[N]}{[J]}\right)^{1/2}C^{\,I\ N\ F}_{\bar{n}_I\ n\ \bar{f}=\bar{n}_I+n}\,|\{j\}\{\tilde{\bar{k}}\}^{F^p}_{f,\,\bar{f}=n+\bar{n}_I}\rangle\,, \tag{2.17}$$

where $[N]=2N+1$ and $[J]=2J+1$. Two examples of this relation are

$$\left|N^p\ \begin{array}{|c|c|}\hline 1&2\\\hline 3\\\cline{1-1}\end{array}\ F=N+1/2\right\rangle=\left(\frac{N+n+1}{2N+2}\right)^{1/2}\left|\begin{array}{|c|c|}\hline 1&2\\\hline 3\\\cline{1-1}\end{array}\ \uparrow\uparrow\ F=N+1/2\ ;\ \downarrow\ \ f,\bar{f}=n+1/2\right\rangle-\left(\frac{N-n+1}{2N+2}\right)^{1/2}\left|\begin{array}{|c|c|}\hline 1&2\\\hline 3\\\cline{1-1}\end{array}\ \uparrow\downarrow\ F=N+1/2\ ;\ \downarrow\ \ f,\bar{f}=n-1/2\right\rangle,$$

$$\left|N^p\ \begin{array}{|c|c|}\hline 1&2\\\hline 3\\\cline{1-1}\end{array}\ F=N-1/2\right\rangle=\left(\frac{N-n}{2N}\right)^{1/2}\left|\begin{array}{|c|c|}\hline 1&2\\\hline 3\\\cline{1-1}\end{array}\ \uparrow\uparrow\ F=N-1/2\ ;\ \downarrow\ \ f,\bar{f}=n+1/2\right\rangle+\left(\frac{N+n}{2N}\right)^{1/2}\left|\begin{array}{|c|c|}\hline 1&2\\\hline 3\\\cline{1-1}\end{array}\ \uparrow\downarrow\ F=N-1/2\ ;\ \downarrow\ \ f,\bar{f}=n-1/2\right\rangle. \tag{2.18}$$

It is important to note that as the cluster approximation is approached, i.e., as n approaches N and both become large, the "off-diagonal" parts of this relation become less significant. Then the lab spin state $\left|\begin{array}{|c|c|}\hline 1&2\\\hline 3\\\cline{1-1}\end{array}\ ,F=N+1/2\right\rangle$ is practically the same as the body spin "up" state $\left|\begin{array}{|c|c|}\hline 1&2\\\hline 3\\\cline{1-1}\end{array}\ \uparrow\uparrow\ ;\ \downarrow\right\rangle$ while $\left|\begin{array}{|c|c|}\hline 1&2\\\hline 3\\\cline{1-1}\end{array}\ ,F=N-1/2\right\rangle$ is very nearly equal to the body spin "down" state $\left|\begin{array}{|c|c|}\hline 1&2\\\hline 3\\\cline{1-1}\end{array}\ \downarrow\downarrow\ ;\ \downarrow\right\rangle$.

One should also note that Eq. (2.18) is not an orthogonal transformation. Instead the inverse of Eq. (2.17) is

$$|\{j\}\{\tilde{\bar{k}}\}^{F^p}_{f,\,\bar{f}=n+\bar{n}_I}\rangle=\sum_{N}\left(\frac{[N]}{[J]}\right)^{1/2}C^{\,I\ N\ F}_{\bar{n}_I\ n\ \bar{f}=\bar{n}_I+n}\,|{}^{N^p}_{n}\{j\}^{F^p}_{f}\rangle\,, \tag{2.19}$$

and this involves a sum over different N for the same F. An example of an orthogonal transformation is given.

$$T=\begin{array}{c|cc}
 & \left|\begin{array}{|c|c|}\hline 1&2\\\hline 3\\\cline{1-1}\end{array}\ \uparrow\uparrow\ F=N+1/2\ ;\ \downarrow\ \ f,\bar{f}=n+1/2\right\rangle & \left|\begin{array}{|c|c|}\hline 1&2\\\hline 3\\\cline{1-1}\end{array}\ \uparrow\downarrow\ F=N+1/2\ ;\ \downarrow\ \ f,\bar{f}=n-1/2\right\rangle \\
\left\langle N\ \begin{array}{|c|c|}\hline 1&2\\\hline 3\\\cline{1-1}\end{array}\ F=N+1/2\right\vert & \left(\frac{N+n+1}{2N+2}\right)^{1/2} & -\left(\frac{N-n+1}{2N+2}\right)^{1/2} \\
\left\langle N+1\ \begin{array}{|c|c|}\hline 1&2\\\hline 3\\\cline{1-1}\end{array}\ F=N+1/2\right\vert & \left(\frac{N-n+1}{2N+2}\right)^{1/2} & \left(\frac{N+n+1}{2N+2}\right)^{1/2}
\end{array} \tag{2.20}$$

TABLE II. Spin frame relations for angular momentum $I=\frac{3}{2}$.

	$\left\vert \begin{array}{|c|}\hline 1\\\hline 2\\\hline 3\\\cline{1-1}\end{array}\ \bar{\uparrow}\,\bar{\uparrow}\,\uparrow \right\rangle$	$\left\vert \begin{array}{|c|}\hline 1\\\hline 2\\\hline 3\\\cline{1-1}\end{array}\ \bar{\uparrow}\,\bar{\uparrow}\,\downarrow \right\rangle$
$\left\langle N\ \begin{array}{|c|}\hline 1\\\hline 2\\\hline 3\\\cline{1-1}\end{array}\ F=N+3/2 \right\vert$	$\left(\frac{(N+n+1)(N+n+2)(N+n+3)}{(2N+2)(2N+3)(2n+4)}\right)^{1/2}$	$\left(\frac{3(N+n+1)(N+n+2)(N-n+1)}{(2N+2)(2N+3)(2N+4)}\right)^{1/2}$
$F=N+1/2\vert$	$\left(\frac{3(N+n+1)(N+n+2)(N-n)}{2N(2N+2)(2N+3)}\right)^{1/2}$	$\left(\frac{(N-3n)(N-3n)(N+n+1)}{2N(2N+2)(2N+3)}\right)^{1/2}$
$F=N-1/2\vert$	$\left(\frac{3(N-n-1)(N-n)(N+n+1)}{(2N-1)(2N)(2N+2)}\right)^{1/2}$	$-\left(\frac{(N+3n+1)(N+3n+1)(N-n)}{(2N-1)2N(2N+2)}\right)^{1/2}$
$F=N-3/2\vert$	$\left(\frac{(N-n-2)(N-n-1)(N-n)}{(2N-2)(2N-1)(2N)}\right)^{1/2}$	$-\left(\frac{3(N-n-1)(N-n)(N+n)}{(2N-2)(2N-1)2N}\right)^{1/2}$

Normally, one is not concerned about states of different N in the elementary cluster approximations. Tables I and II give the desired frame transformation relations between XY_3 states of the same N and n but different $F=N+\Delta$ ($\Delta=\pm\frac{1}{2},\frac{3}{2}$). Table I is a repeat of Eq. (2.18).

One should note that the permutational properties of orbit-spin states such as

$$\left|\begin{array}{|c|c|}\hline 1&2\\\hline 3\\\cline{1-1}\end{array}\ \uparrow\uparrow\ \downarrow\right\rangle \text{ or } \left|\begin{array}{|c|c|}\hline 1&2\\\hline 3\\\cline{1-1}\end{array}\ \downarrow\downarrow\ \downarrow\right\rangle$$

do not depend on whether the spins are quantized in the lab frame or in the body frame. The assembly formula (Fig. 5) can be used to write

$$\left|\begin{array}{|c|c|}\hline 1&2\\\hline 3\\\cline{1-1}\end{array}\ \downarrow\downarrow\ \downarrow\right\rangle$$

in terms of body-frame Slater states

$$\left|\begin{array}{l}1\downarrow\\2\uparrow\\3\downarrow\end{array}\right\rangle,\ \left|\begin{array}{l}1\downarrow\\2\downarrow\\3\uparrow\end{array}\right\rangle,\ \text{and}\ \left|\begin{array}{l}1\downarrow\\2\uparrow\\3\uparrow\end{array}\right\rangle$$

just the same as in the lab frame. Indeed, body-frame Slater states are convenient bases for beginning construction of Hamiltonian matrices as seen in Sec. II D.

D. Methods for solving spin rotation Hamiltonians

Rather than giving a complete description of all relevant spin rotation Hamiltonians we shall pick examples from the collection of operators given in the literature[29,30] which are sufficiently complex to demonstrate the method for setting up matrices in the cluster bases. Then the resulting matrices will be solved in order to show the physical properties of the states in various cases. One operator example is the tensor-spin-rotation operator

$$H_{\rm tsr}=T\sum_{j,\,k=a,b,c}[\vec{\mathrm{r}}(k)-\vec{\mathrm{r}}(j)]\times[a\vec{\mathrm{v}}(k)-\vec{\mathrm{v}}(j)]\cdot\vec{\mathrm{I}}(k)\,, \tag{2.21}$$

which represents the interaction between the spin of nucleus (k) at position $\vec{\mathrm{r}}(k)$ and the velocity $\vec{\mathrm{v}}(j)$ of charge around nucleus (j) at position $\vec{\mathrm{r}}(j)$. The coefficient a is meant to account for Thomas precession. Following Ref. 29 one expresses the velocity in terms of angular velocity $(\vec{\omega})$ and momentum $(\vec{\mathrm{N}})$ of the frame, i.e., let

$$\vec{\mathrm{v}}(k)=\vec{\omega}\times\vec{\mathrm{r}}(k)\,,\qquad \omega_{\bar{x}}=2A\,\bar{N}_x,\quad \omega_{\bar{y}}=2B\bar{N}_y,\quad \omega_{\bar{z}}=2C\bar{N}_z\,, \tag{2.22}$$

where A, B, and C are the prinicpal molecular rotation constants. (Two of these must be equal in first approximation for an XY_3 molecule. If we consider twofold axial rotation as in Fig. 2, then $B=C$.) Then the Hamiltonian becomes

$$H_{\rm tsr}=T\sum_{j,k}(\vec{\omega}\{[\vec{\mathrm{r}}(j)-a\,\vec{\mathrm{r}}(k)]\cdot[\vec{\mathrm{r}}(j)-\vec{\mathrm{r}}(k)]\}-[\vec{\mathrm{r}}(j)-a\,\vec{\mathrm{r}}(k)][(\vec{\mathrm{r}}(j)-\vec{\mathrm{r}}(k))\cdot\vec{\omega}])\cdot\vec{\mathrm{I}}(k)\,, \tag{2.23}$$

In most elementary cluster approximations (ECA) one need consider only terms involving the $\bar{z}$ component of $\vec{\omega}$ or $\vec{\mathrm{N}}$. The remaining terms are

$$H_{\rm tsr}(\mathrm{ECA})=2CT\sum_{j,k}\bar{N}_z(\bar{I}_z(k)\{[x(j)-x(k)][x(j)-ax(k)]+[y(j)-y(k)][y(j)-ay(k)]\}-[z(j)-z(k)]\{\bar{I}_x(k)[x(j)-ax(k)]+\bar{I}_y(k)[y(j)-ay(k)]\})\,, \tag{2.24}$$

Table II. (*Continued*).

	$\left\langle N\ \begin{array}{|c|}\hline 1\\\hline 2\\\hline 3\\\cline{1-1}\end{array}\ f\right\rangle$	$\left\langle n\ \begin{array}{|c|}\hline 1\\\hline 2\\\hline 3\\\cline{1-1}\end{array}\ f\right\rangle$
	$\left\langle\begin{array}{|c|}\hline 1\\\hline 2\\\hline 3\\\cline{1-1}\end{array}\ \uparrow\downarrow\downarrow\right\rangle$	$\left\langle\begin{array}{|c|}\hline 1\\\hline 2\\\hline 3\\\cline{1-1}\end{array}\ \downarrow\downarrow\downarrow\right\rangle$
$F=N+1/2$	$-\left(\frac{(N+3n)(N+3n)(N-n)}{2N(2N+2)(2N+3)}\right)^{1/2}$	$\left(\frac{3(N-n+1)(N-n+2)(N+n)}{2N(2N+2)(2N+3)}\right)^{1/2}$
$F=N-1/2$	$\left(\frac{(N-3n+1)(N-3n+1)(N+n)}{(2N-1)2N(2N+2)}\right)^{1/2}$	$-\left(\frac{3(N+n-1)(N+n)(N-n+1)}{(2N-1)(2N)(2N+2)}\right)^{1/2}$
$F=N-3/2$	$-\left(\frac{3(N+n-1)(N+n)(N-n)}{(2N-2)(2N-1)2N}\right)^{1/2}$	$\left(\frac{(N+n-2)(N+n-1)(N+n)}{(2N-2)(2N-1)2N}\right)^{1/2}$

where now all operators are expressed in the body frame. For the XY_3 molecule stuck on two-fold axes [see Fig. 2(a)] the following form of H_{tsr}(ECA) results:

$$H_{tsr}(\text{ECA on 2}) = \bar{N}_z\{\alpha\bar{I}_z(c)+\beta[\bar{I}_z(a)+\bar{I}_z(b)] + \gamma\bar{I}_y(c)+\delta[-I_x(a)+I_x(b)] + \epsilon[I_y(a)+I_y(b)]+\text{permutations}\}, \quad (2.25)$$

where $\alpha, \beta, \ldots$, etc., depend upon the geometry of the XY_3 molecule, the molecular constant C, and the Hamiltonian parameter T.

When evaluating this Hamiltonian in a Slater body-spin bases

$$\left\{\left|\begin{matrix}1\bar{\uparrow}\\2\bar{\uparrow}\\3\bar{\uparrow}\end{matrix}\right\rangle, \left|\begin{matrix}1\bar{\uparrow}\\2\bar{\uparrow}\\3\bar{\downarrow}\end{matrix}\right\rangle, \ldots, \text{etc.}\right\},$$

it is convenient to imagine that nuclei a, b, and c are in states 1, 2, and 3, respectively, as in Fig. 2(a). In this way one can ignore the equivalent parts of a Hamiltonian operator such as Eq. (2.25) which differ only by permutation of identical nuclei. The resulting Hamiltonian matrix is given below.

$$\langle H_{tsr}\rangle = \begin{array}{c|cccccccc} & \left|\begin{matrix}1\bar{\uparrow}\\2\bar{\uparrow}\\3\bar{\uparrow}\end{matrix}\right\rangle & \left|\begin{matrix}1\bar{\uparrow}\\2\bar{\uparrow}\\3\bar{\downarrow}\end{matrix}\right\rangle & \left|\begin{matrix}1\bar{\uparrow}\\2\bar{\downarrow}\\3\bar{\uparrow}\end{matrix}\right\rangle & \left|\begin{matrix}1\bar{\downarrow}\\2\bar{\uparrow}\\3\bar{\uparrow}\end{matrix}\right\rangle & \left|\begin{matrix}1\bar{\uparrow}\\2\bar{\downarrow}\\3\bar{\downarrow}\end{matrix}\right\rangle & \left|\begin{matrix}1\bar{\downarrow}\\2\bar{\uparrow}\\3\bar{\downarrow}\end{matrix}\right\rangle & \left|\begin{matrix}1\bar{\downarrow}\\2\bar{\downarrow}\\3\bar{\uparrow}\end{matrix}\right\rangle & \left|\begin{matrix}1\bar{\downarrow}\\2\bar{\downarrow}\\3\bar{\downarrow}\end{matrix}\right\rangle \\ \hline \left|\begin{matrix}1\bar{\uparrow}\\2\bar{\uparrow}\\3\bar{\uparrow}\end{matrix}\right\rangle & \alpha n/2+\beta n & \gamma n/2i & (\delta-i\epsilon)n/2 & -(\delta+i\epsilon)n/2 & 0 & 0 & 0 & 0 \\ \left|\begin{matrix}1\bar{\uparrow}\\2\bar{\uparrow}\\3\bar{\downarrow}\end{matrix}\right\rangle & & \beta n-\alpha n/2 & 0 & 0 & (\delta-i\epsilon)n/2 & -(\delta+i\epsilon)n/2 & 0 & 0 \\ \left|\begin{matrix}1\bar{\uparrow}\\2\bar{\downarrow}\\3\bar{\uparrow}\end{matrix}\right\rangle & & & \alpha n/2 & 0 & \gamma n/2i & 0 & -(\delta+i\epsilon)n/2 & 0 \\ \left|\begin{matrix}1\bar{\downarrow}\\2\bar{\uparrow}\\3\bar{\uparrow}\end{matrix}\right\rangle & & & & \alpha n/2 & 0 & \gamma n/2i & (\delta-i\epsilon)n/2 & 0 \\ \left|\begin{matrix}1\bar{\uparrow}\\2\bar{\downarrow}\\3\bar{\downarrow}\end{matrix}\right\rangle & & & & & -\alpha n/2 & 0 & 0 & -(\delta+i\epsilon)n/2 \\ \left|\begin{matrix}1\bar{\downarrow}\\2\bar{\uparrow}\\3\bar{\downarrow}\end{matrix}\right\rangle & & & & & & -\alpha n/2 & 0 & (\delta-i\epsilon)n/2 \\ \left|\begin{matrix}1\bar{\downarrow}\\2\bar{\downarrow}\\3\bar{\uparrow}\end{matrix}\right\rangle & & & & & & & \alpha n/2-\beta n & \gamma n/2i \\ \left|\begin{matrix}1\bar{\downarrow}\\2\bar{\downarrow}\\3\bar{\downarrow}\end{matrix}\right\rangle & & & & & & & & -\alpha n/2-\beta n \end{array} \quad (2.26)$$

Let us solve the preceding Hamiltonian matrix with only the constants $\alpha = 2h/n$, $\beta = k/n$, and the rest zero. Using the assembly formula this can be reexpressed in the orbit-body-spin basis as follows.

$$\langle H'_{sr}\rangle = \begin{array}{c|cccccccc} & \left|\begin{matrix}1\\2\\3\end{matrix}\,\bar{\uparrow}\bar{\uparrow}\bar{\uparrow}\right\rangle & \left|\begin{matrix}1&2\\3\end{matrix}\,\bar{\uparrow}\bar{\uparrow}\bar{\downarrow}\right\rangle & \left|\begin{matrix}1&3\\2\end{matrix}\,\bar{\uparrow}\bar{\uparrow}\bar{\downarrow}\right\rangle & \left|\begin{matrix}1\\2\\3\end{matrix}\,\bar{\uparrow}\bar{\uparrow}\bar{\downarrow}\right\rangle & \left|\begin{matrix}1&2\\3\end{matrix}\,\bar{\uparrow}\bar{\downarrow}\bar{\uparrow}\right\rangle & \left|\begin{matrix}1&3\\2\end{matrix}\,\bar{\uparrow}\bar{\downarrow}\bar{\downarrow}\right\rangle & \left|\begin{matrix}1\\2\\3\end{matrix}\,\bar{\uparrow}\bar{\downarrow}\bar{\downarrow}\right\rangle & \left|\begin{matrix}1\\2\\3\end{matrix}\,\bar{\downarrow}\bar{\downarrow}\bar{\downarrow}\right\rangle \\ \hline \left|\begin{matrix}1\\2\\3\end{matrix}\,\bar{\uparrow}\bar{\uparrow}\bar{\uparrow}\right\rangle & h+k & \cdots & \cdots & \cdots & \cdots & \cdots & \cdots & \cdots \\ \left|\begin{matrix}1&2\\3\end{matrix}\,\bar{\uparrow}\bar{\uparrow}\bar{\downarrow}\right\rangle & & h & 0 & 0 & \cdots & \cdots & \cdots & \cdots \\ \left|\begin{matrix}1&3\\2\end{matrix}\,\bar{\uparrow}\bar{\uparrow}\bar{\downarrow}\right\rangle & & 0 & (2k-h)/3 & \sqrt{2}(2h-k)/3 & \cdots & \cdots & \cdots & \cdots \\ \left|\begin{matrix}1\\2\\3\end{matrix}\,\bar{\uparrow}\bar{\uparrow}\bar{\downarrow}\right\rangle & & 0 & \sqrt{2}(2h-k)/3 & (h+k)/3 & \cdots & \cdots & \cdots & \cdots \\ \left|\begin{matrix}1&2\\3\end{matrix}\,\bar{\uparrow}\bar{\downarrow}\bar{\uparrow}\right\rangle & & & & & -h & 0 & 0 & \cdots \\ \left|\begin{matrix}1&3\\2\end{matrix}\,\bar{\uparrow}\bar{\downarrow}\bar{\downarrow}\right\rangle & & & & & 0 & (h-2k)/3 & \sqrt{2}(2h-k)/3 & \cdots \\ \left|\begin{matrix}1\\2\\3\end{matrix}\,\bar{\uparrow}\bar{\downarrow}\bar{\downarrow}\right\rangle & & & & & 0 & \sqrt{2}(2h-k)/3 & -(h+k)/3 & \cdots \\ \left|\begin{matrix}1\\2\\3\end{matrix}\,\bar{\downarrow}\bar{\downarrow}\bar{\downarrow}\right\rangle & & & & & & & & -h-k \end{array} \quad (2.27)$$

The desired submatrices of the total Hamiltonian

$$H = H_{\text{centrifugal}} + H'_{sr}$$

are obtained by first converting the $\langle H'_{sr}\rangle$ to block diagonal form using the frame transformation relations in Tables I and II, and then inserting the centrifugal tunneling eigenvalues $H^{\pm} \pm 2S$, $H^{\pm} \pm S$, etc., from Fig. 3 in the appropriate diagonal positions of each submatrix. For example the first block corresponding to total momentum $F^{\rho} = (N+\frac{3}{2})^{\pm}$ is a 1×1 block of value

$$\left\langle \left|\begin{matrix}1\\2\\3\end{matrix}\right| (N+\tfrac{3}{2})^{\pm} \middle| H \middle| \left|\begin{matrix}1\\2\\3\end{matrix}\right| (N+\tfrac{3}{2})^{\pm} \right\rangle = H^{\pm} \pm 2S + b_{11}^2(h+k) + \tfrac{1}{3}b_{12}^2(h+k) - \tfrac{1}{3}b_{13}^2(h+k) - b_{14}^2(h+k) \quad (2.28)$$

where b_{ij} is the (ij)th entry in Table II. Note that only the first three terms of Eq. (2.28) exist in the limit of high N and n. Note the difference between positive and negative parity states $\left|\begin{array}{|c|}\hline 1\\\hline 2\\\hline 3\\\hline\end{array}\,(N+\tfrac{3}{2})^{\pm}\right\rangle$. The centrifugal part changes from $(H^{+}+2S)$ to $(H^{-}-2S)$. [Recall Fig. 3(c).]

The second block is a 3×3 matrix corresponding to the three states having $F^{p}=(N+\frac{1}{2})^{p}$. We have

$$\langle H\rangle^{F^{p}=(N+1/2)^{\pm}}=\begin{array}{c}\left|\begin{array}{|c|c|}\hline 1&2\\\hline 3\\\cline{1-1}\end{array}\,(N+1/2)^{\pm}\right\rangle \quad \left|\begin{array}{|c|c|}\hline 1&3\\\hline 2\\\cline{1-1}\end{array}\,(N+1/2)^{\pm}\right\rangle \quad \left|\begin{array}{|c|}\hline 1\\\hline 2\\\hline 3\\\hline\end{array}\,(N+1/2)^{\pm}\right\rangle\\ \left|\begin{array}{ccc} H^{\pm}\pm S+a_{11}^{2}h & 0 & 0\\ -a_{12}^{2}h & & \\ 0 & H^{\pm}\mp S+a_{11}^{2}(2k-h)/3 & -a_{11}b_{22}\sqrt{2}(2h-k)/3\\ & +a_{12}^{2}(h-2k)/3 & -a_{12}b_{23}\sqrt{2}(2h-k)/3\\ 0 & -a_{11}b_{22}\sqrt{2}(2h-k)/3 & H^{\pm}\pm 2S+b_{22}^{2}(h+k)/3\\ & -a_{12}b_{23}\sqrt{2}(2h-k)/3 & +b_{21}^{2}(h+k)-b_{23}^{2}(h+k)/3\\ & & -b_{24}^{2}(h+k)\end{array}\right|\end{array} \tag{2.29}$$

where a_{ij} is the (ij)th entry in Table I. Note that in the limit that $a_{ij}=\delta_{ij}=b_{ij}$ the angular momentum blocks approach those in the orbit-body-spin representation of Eq. (2.27). The same applies to the remaining blocks given in the following two equations.

$$\langle H\rangle^{F^{p}=(N-1/2)^{\pm}}=\begin{array}{c}\left|\begin{array}{|c|c|}\hline 1&2\\\hline 3\\\cline{1-1}\end{array}\,(N-1/2)^{\pm}\right\rangle \quad \left|\begin{array}{|c|c|}\hline 1&3\\\hline 2\\\cline{1-1}\end{array}\,(N-1/2)^{\pm}\right\rangle \quad \left|\begin{array}{|c|}\hline 1\\\hline 2\\\hline 3\\\hline\end{array}\,(N-1/2)^{\pm}\right\rangle\\ \left|\begin{array}{ccc} H^{\pm}\pm S-a_{22}^{2}h & 0 & 0\\ +a_{21}^{2}h & & \\ 0 & H^{\pm}\mp S+a_{22}^{2}(h-2k)/3 & -a_{22}b_{33}\sqrt{2}(2h-k)/3\\ & +a_{21}^{2}(2k-h)/3 & -a_{21}b_{32}\sqrt{2}(2h-k)/3\\ 0 & -a_{22}b_{33}\sqrt{2}(2h-k)/3 & H^{\pm}\pm 2S-b_{33}^{2}(h+k)/3\\ & -a_{21}b_{32}\sqrt{2}(2h-k)/3 & +b_{32}^{2}(h+k)/3-b_{34}^{2}(h+k)\\ & & +b_{31}^{2}(h+k)\end{array}\right|\end{array} \tag{2.30}$$

$$\left\langle\begin{array}{|c|}\hline 1\\\hline 2\\\hline 3\\\hline\end{array}\,(N-3/2)^{\pm}\left|H\right|\begin{array}{|c|}\hline 1\\\hline 2\\\hline 3\\\hline\end{array}\,(N-3/2)^{\pm}\right\rangle=H^{\pm}\pm 2S-b_{44}^{2}(h+k)+b_{41}^{2}(h+k)+\tfrac{1}{3}b_{42}^{2}(h+k)-\tfrac{1}{3}b_{43}^{2}(h+k)\,. \tag{2.31}$$

The zero components in the off-diagonal parts of (2.29) and (2.30) are nonzero for a general spin-rotational Hamiltonian.

In Fig. 6 the eigenvalues of the centrifugal and spin-rotation Hamiltonian matrices [Eqs. (2.28)–(2.31)] are plotted as functions of the centrifugal tunneling parameter S for fixed hyperfine parameters $h=2$ and $k=5$. The high-momentum approximation $a_{ij}=\delta_{ij}=b_{ij}$ is assumed. Also the normal inversion splitting is set equal to zero, i.e., we assume $H^{+}=H^{-}$.

Despite this, there is still a splitting between even and odd parity states $(N\pm\frac{1}{2})^{+}$ and $(N\pm\frac{1}{2})^{-}$ due just to hyperfine interactions, as seen in Fig. 6(a). Even if the mass or body of the nuclei do not undergo improper operations their spin states may still be "traded." The effect is a splitting between $\begin{array}{|c|c|}\hline 1&2\\\hline 3\\\cline{1-1}\end{array}$ and $\begin{array}{|c|c|}\hline 1&3\\\hline 2\\\cline{1-1}\end{array}$ tableau states that is similar though not identical to "normal" inversion splitting.

The complicated region of low centrifugal cluster splitting ($S<4$) is plotted in the enlarged Fig. 6(b). This corresponds to the beginning of case (2) in which the hyperfine splittings are larger than those of the centrifugal cluster. Entering this region on the right-hand side of Fig. 6(b) are energy trajectories labeled by body defined orbit-spin tableaus described in the preceding Secs. II and III. Certain of these states mix strongly to form new

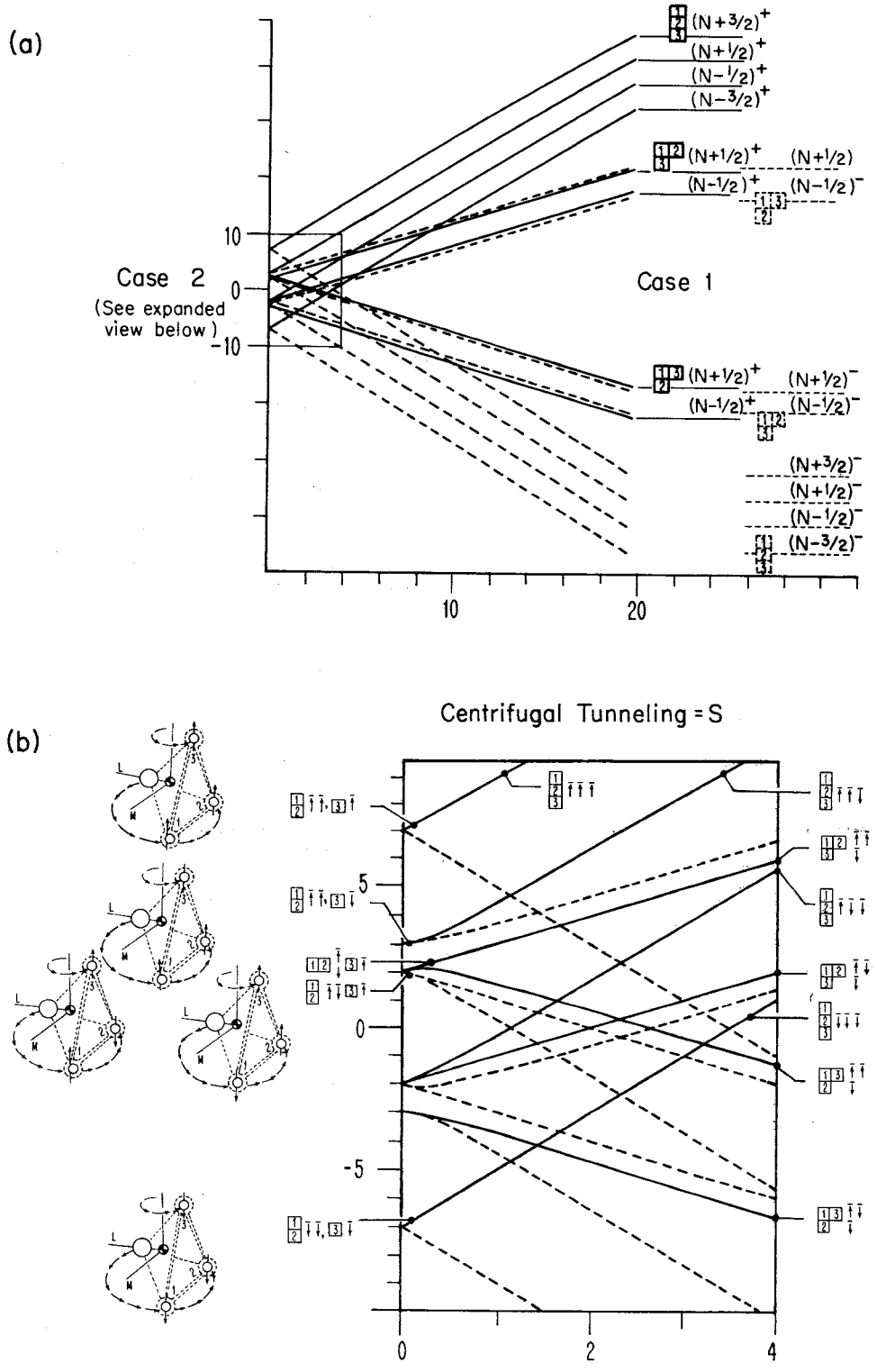

FIG. 6. XY_3 superhyperfine correlation between cases (1) and (2) for twofold level cluster. (a) Case (1); (b) case (2). Energy levels obtained from (2.28)–(2.31) are plotted as a function of the cluster tunneling parameter (S) for fixed pseudospin rotation parameters $h=2$ and $k=5$. The high-momentum spin frame relations $a_{ij}=\delta_{ij}=b_{ij}$ are used, and "real" inversion splitting is assumed zero ($H^+=H^-$).

eigenstates in the limit of case (2) as indicated on the left-hand side of Fig. 6(b). For example, $\left|\begin{smallmatrix}1\\2\\3\end{smallmatrix}\uparrow\uparrow\downarrow\right\rangle$ and $\left|\begin{smallmatrix}1&3\\2\end{smallmatrix}\uparrow\uparrow\downarrow\right\rangle$ mix strongly to make eigenvectors of the Hamiltonian submatrix in Eq. (2.27). Using Slater determinant notation the hyperfine eigenstates have the following form: the state

$$\left|\begin{smallmatrix}1\uparrow\\2\uparrow\\3\downarrow\end{smallmatrix}\right\rangle=-\left(\frac{2}{3}\right)^{1/2}\left|\begin{smallmatrix}1&3\\2\end{smallmatrix}\uparrow\uparrow\downarrow\right\rangle+\left(\frac{1}{3}\right)^{1/2}\left|\begin{smallmatrix}1\\2\\3\end{smallmatrix}\uparrow\uparrow\downarrow\right\rangle \tag{2.32}$$

has energy $k-h$ and the state

$$\frac{1}{\sqrt{2}}\left|\begin{smallmatrix}1\uparrow\\2\downarrow\\3\uparrow\end{smallmatrix}\right\rangle+\frac{1}{\sqrt{2}}\left|\begin{smallmatrix}1\downarrow\\2\uparrow\\3\uparrow\end{smallmatrix}\right\rangle=\left(\frac{1}{3}\right)^{1/2}\left|\begin{smallmatrix}1&3\\2\end{smallmatrix}\uparrow\uparrow\downarrow\right\rangle+\left(\frac{2}{3}\right)^{1/2}\left|\begin{smallmatrix}1\\2\\3\end{smallmatrix}\uparrow\uparrow\downarrow\right\rangle \tag{2.33}$$

has energy h. The latter ends up being degenerate with the state

$$\frac{1}{\sqrt{2}}\left|\begin{smallmatrix}1\uparrow\\2\downarrow\\3\uparrow\end{smallmatrix}\right\rangle-\frac{1}{\sqrt{2}}\left|\begin{smallmatrix}1\downarrow\\2\uparrow\\3\uparrow\end{smallmatrix}\right\rangle=\left|\begin{smallmatrix}1&2\\3\end{smallmatrix}\uparrow\uparrow\downarrow\right\rangle \tag{2.34}$$

which is free from any mixing due to the Hamiltonian being studied here. [Note that $\left|\begin{smallmatrix}1&2\\3\end{smallmatrix}\uparrow\uparrow\downarrow\right\rangle$ is associated with a straight-line energy trajectory in Fig. 6(b).]

In the limit of case (2) the molecule becomes stuck on a single twofold axis. The nucleus stranded in state $|3\rangle$ on the apex of the triangle is prohibited from ever trading with any of the nuclei in states $|1\rangle$ or $|2\rangle$ rotating around with the base of the triangle. The case (2) hyperfine eigenfunctions [Eqs. (2.32)–(2.34)] have precisely the form that one gets by excluding the nucleus in the third state from orbital symmetrization. By using the assembly formula (Fig. 5) or Eq. (2.13) one finds the following equivalent expressions for the hyperfine eigenfunctions in which only the particles in the first and second states are symmetrized

$$\begin{aligned}\frac{1}{\sqrt{2}}\left|\begin{smallmatrix}1\uparrow\\2\downarrow\\3\uparrow\end{smallmatrix}\right\rangle-\frac{1}{\sqrt{2}}\left|\begin{smallmatrix}1\downarrow\\2\uparrow\\3\uparrow\end{smallmatrix}\right\rangle&=\left\{\frac{1}{\sqrt{2}}\left|\begin{smallmatrix}1\uparrow\\2\downarrow\end{smallmatrix}\right\rangle-\frac{1}{\sqrt{2}}\left|\begin{smallmatrix}1\downarrow\\2\uparrow\end{smallmatrix}\right\rangle\right\}|3\uparrow\rangle\\&=\left|\begin{smallmatrix}1&2\\\downarrow\end{smallmatrix}\uparrow\right\rangle|3\uparrow\rangle,\\\frac{1}{\sqrt{2}}\left|\begin{smallmatrix}1\uparrow\\2\downarrow\\3\uparrow\end{smallmatrix}\right\rangle+\frac{1}{\sqrt{2}}\left|\begin{smallmatrix}1\downarrow\\2\uparrow\\3\uparrow\end{smallmatrix}\right\rangle&=\left|\begin{smallmatrix}1\\2\end{smallmatrix}\uparrow\downarrow\right\rangle|3\uparrow\rangle,\end{aligned} \tag{2.35}$$

$$\left|\begin{smallmatrix}1\uparrow\\2\uparrow\\3\downarrow\end{smallmatrix}\right\rangle=\left|\begin{smallmatrix}1\\2\end{smallmatrix}\uparrow\uparrow\right\rangle|3\downarrow\rangle.$$

This is the origin of the "broken tableau" notation used to denote the case (2) states on the left-hand side of Fig. 6. Note that similar arguments can be used for the analogous "down spin" cases in the lower half of Fig. 6(b) as well as the negative-parity states indicated by dotted lines in the figure.

By including the off-diagonal a_{ij} and b_{ij} frame transformation coefficients one obtains effects of the spins "slipping" in the body frame. This may be particularly important if the other hyperfine terms belonging to coefficients γ, δ, and ϵ in Eqs. (2.25) and (2.26) are to be included also. Roughly speaking, these terms tend to cause the spins to "cant," i.e., line up with directions which slope away from the body rotation axis (N) and lie instead along the internal molecular magnetic field.

III. ROTATIONAL CLUSTER AND NUCLEAR SPIN STATES IN XY_4 MOLECULES

The methods introduced in Sec. II by way of the XY_3 molecular example will now be applied to the cluster states of the tetrahedral (XY_4) molecule. The fourfold clusters [see the left-hand two-thirds of Figs. 1(c) and 1(d)] are the most common ones. Also, they require slightly more complicated algebra for the hyperfine theory. In addition, they generally have the smallest superfine splittings and so more fourfold than threefold clusters will fall into case (2). Hence, we shall concentrate our analysis on fourfold clusters.

However, the ground vibronic states of heavy tetrahedral molecules (CF_4, SiF_4, etc.) have even finer fine structure than the excited states and correspondingly smaller superfine splittings. Therefore, we expect to find more case (2) clusters there including many more of the threefold variety. Also, some of the light tetrahedral molecules (CH_4, SiH_4, GeH_4, CD_4,...) have significant amounts of a sixth-rank centrifugal distortion perturbation, and this relative contribution grows with J roughly as $J^6/J^4=J^2$. If the sixth-rank contribution is positive as it is in ν_3 (3.39 μm) in CH_4 then the effect is to produce more abnormally tight and even degenerate fourfold clusters at the expense of the threefold clusters.[36] (Extraordinary cluster spectra can occur even at low J. Even twofold clusters appear.) However, if the sixth-rank contribution is negative the number of threefold clusters may grow at the expense of the fourfold ones. Then some rather unusual cases can arise which are outside of the scope of this article.

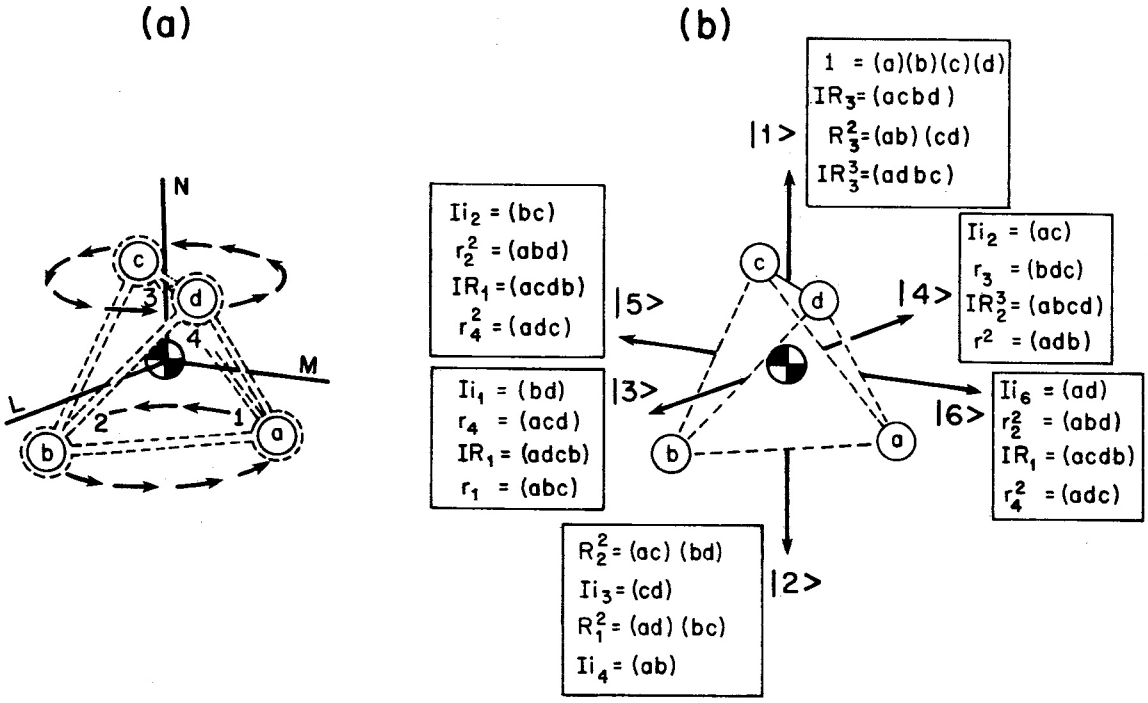

FIG. 7. XY_4 molecule in fourfold axial rotational states. (a) Y particles are labeled by letters and states by numbers as in Fig. 2(a); (b) each coset of tetrahedral symmetry operations or permutations corresponds to a different direction for the fourfold rotation axis (N) with respect to the Y nuclei, and to a different cluster base state $|1\rangle$, $|2\rangle$, ..., $|6\rangle$.

A. Fourfold cluster bases

As explained in Ref. 3 fourfold clusters are associated with rapid rotation around fourfold (C_{4i}) symmetry axes as shown in Fig. 7(a). The cluster splitting is due to tunneling of the angular momentum vector between the six different fourfold axes indicated in Fig. 7(b). Roughly two types of fourfold clusters exist depending on the cluster momentum component n. If n is odd the clusters have a $T_1 \oplus T_2$ doublet structure, while if n is even they are triplets: $A_2 \oplus T_2 \oplus E$ if $n=2$ mod 4, and $A_1 \oplus T_1 \oplus E$ if $n=0$ mod 4. We shall concentrate on the $A_1 \oplus T_1 \oplus E$ triplets.

1. $O_4 \uparrow O = A_1 \oplus T_1 \oplus E$ clusters

As explained in Ref. 3 the six cluster states for $n=0$ mod 4 form the basis of an induced representation $O_4 \uparrow O$ which reduces to three irreducible components. There is the single component A_1 of tunneling energy $(H-4S)$, the triply degenerate component T_1 of energy (H), and the doubly degenerate component E of energy $(H+2S)$. We shall review the structure and meaning of the induced representation and its reduction by critically examining the projection operators in Eq. (2.4) as they apply to this problem. Before we begin, note that the 2:1 superfine cluster splitting[3] is a result of having only "nearest-neighbor" tunneling amplitudes $(-S)$ between axis states $|1\rangle - |6\rangle$ in Fig. 7(b). Apparently this assumption is correct for fourth rank as well as fourth-plus-sixth rank centrifugal distortion operators.[36]

The desired eigencombinations of states $|1\rangle - |6\rangle$ are obtained by applying permutation or point group projectors $P_{ij}^{[\mu]}$ [recall Eq. (2.4)] to the initial state

$$|1\rangle = |{}^{N\,p}_{m\,n}\,1\rangle \tag{3.1}$$

for which $n=0$ mod 4. In this case, there are four times as many symmetry-group operators as cluster states. Hence each cluster state $|c\rangle$ belongs to a particular "coset" $l_c \cdot (C_{4i})$ of four operations shown next to that state in Fig. 7(b). [In the figure the connection between permutations $(abc\ldots)$ and a previous notation[3] for cubic-tetrahedral point group operations is made.] The sum in Eq. (2.4) over all 24 elements $\bar{r}$ of the tetrahedral group may be shortened to a sum over just one "leader" element l_c chosen arbitrarily from each coset. To achieve this simplification one must examine the sum over just the elements in the invariance subgroup $C_{4i} = \{1, IR_3, R_3^2, IR_3^3\}$ associated with the original state $|1\rangle$ in Fig. 7(b), i.e., the first four terms in projector sum.

$$|{}^{N^p}_{mn}{}^{\{\mu\}}_{\{i\}\{j\}}\rangle = P^{\{\mu\}}_{\{i\}\{j\}}|{}^{N^p}_{mn}1\rangle/\mathfrak{N}^{1/2} = (l^{\{\mu\}}/24\mathfrak{N}^{1/2})\{\mathfrak{D}^{\{\mu\}*}_{\{i\}\{j\}}(1)1 + \mathfrak{D}^{\{\mu\}*}_{\{i\}\{j\}}(I\bar{R}_3)I\bar{R}_3 + \mathfrak{D}^{\{\mu\}*}_{\{i\}\{j\}}(\bar{R}_3^2)\bar{R}_3^2 + \mathfrak{D}^{\{\mu\}*}_{\{i\}\{j\}}(I\bar{R}_3^3)I\bar{R}_3^3\}|1\rangle + \cdots$$
$$= (l^{\{\mu\}}/24\mathfrak{N}^{1/2})\{\mathfrak{D}^{\{\mu\}*}_{\{i\}\{j\}}(1) + (-1)^p\mathfrak{D}^{\{\mu\}*}_{\{i\}\{j\}}(I\bar{R}_3) + \mathfrak{D}^{\{\mu\}*}_{\{i\}\{j\}}(\bar{R}_3^2) + (-1)^p\mathfrak{D}^{\{\mu\}*}_{\{i\}\{j\}}(I\bar{R}_3^3)\}|1\rangle + \cdots$$
$$= (l^{\{\mu\}}/6\mathfrak{N}^{1/2})\mathfrak{D}^{\{\mu\}}_{\{i\}\{j\}}(\tfrac{1}{4}[1 + (-1)^pI\bar{R}_3 + \bar{R}_3^2 + (-1)^pI\bar{R}_3^3])|1\rangle + \cdots . \quad (3.2)$$

In the last two steps Eqs. (2.1) and (2.2) were used with $\alpha = \frac{1}{4}\pi$ and $n = 0 \bmod 4$. Now the trick is to pick only those representations $\mathfrak{D}^{\{\mu\}}(P^c)$ of the invariance subgroup projection operator

$$P^c = \tfrac{1}{4}[1 + (-1)^pI\bar{R}_3 + \bar{R}_3^2 + (-1)^pI\bar{R}_3^3] \quad (3.3)$$

[here $c = (O_4)$] which have diagonal form

$$\mathfrak{D}^{\{\mu\}}(P^c) = \begin{bmatrix} \cdots\ \{j\}\ \cdots & & \\ 0 & \ddots & \\ & \ddots\ 1 & \\ & 0\ \ddots & \\ & & \ddots \end{bmatrix} . \quad (3.4)$$

Then the only surviving eigenstates will be those belonging to $\{j\}$ associated with nonzero or unit components on the diagonal of $\mathfrak{D}^{\{\mu\}}(P^c)$. The diagonal form (3.4) is achieved automatically by any representation that is reduced with respect to the invariance subgroup $\{\cdots \bar{R}_i\}$, i.e., for which

$$\mathfrak{D}^{\{\mu\}}(\bar{R}_i) = \begin{bmatrix} \cdot & & \cdots\{j\}\cdots & \\ & D^a(\bar{R}_i) & 0 & \\ & 0 & D^b(\bar{R}_i) & 0 \\ & & 0 & D^c(\bar{R}_i) \\ & & & \ddots \end{bmatrix} \quad (3.5a)$$

or

$$\mathfrak{D}^{\{\mu\}}\downarrow(\text{invariance subgroup}) = D^a \oplus D^b \oplus D^c \oplus \cdots . \quad (3.5b)$$

It is in this way that the $\{j\}$th components of the eigenstate $|{}^{N^p}_{mn}{}^{\{\mu\}}_{\{i\}\{j\}}\rangle$ are associated with the (c)th induced representation

$$D^c\downarrow(\text{molecular symmetry group}) = \cdots \oplus \mathfrak{D}^{\{\mu\}} \oplus \cdots . \quad (3.6)$$

[Indeed, these observations constitute a direct proof of the Frobenius reciprocity theorem.[37] The theorem states that the number $f^c(\{\mu\}\downarrow(\text{subgroup}))$ of times D^c appears in the reduction of $\mathfrak{D}^{\{\mu\}}$ shall equal the number $f^{\{\mu\}}(c\downarrow(\text{group}))$ of times $\mathfrak{D}^{\{\mu\}}$ appears in the induced representation (3.6).]

For example, the T_d representation E belonging to tableau $\{\mu\} = \{2,2\}$ happens to already be in reduced form with respect to the fourfold axial invariance subgroup. For positive parity $[(-1)^p = 1]$, one finds [here $c = (O_4)$ again]

$$\mathfrak{D}^{[2,2]}(P^c) = \begin{pmatrix} 1 & 0 \\ 0 & 0 \end{pmatrix} , \quad (3.7a)$$

while for negative parity $[(-1)^p = -1]$, one finds

$$\mathfrak{D}^{[2,2]}(P^c) = \begin{pmatrix} 0 & 0 \\ 0 & 1 \end{pmatrix} . \quad (3.7b)$$

Hence the XY_4 E-type "inversion doublet" consists of states

$$\left|{}^{N^+}_{mn}\ \begin{array}{|c|c|}\hline 1&2\\\hline 3&4\\\hline\end{array} F^p = N^+\right\rangle \text{ and } \left|{}^{N^-}_{mn}\ \begin{array}{|c|c|}\hline 1&3\\\hline 2&4\\\hline\end{array} F^p = N^-\right\rangle .$$

The total spin of the conjugate spin tableau state $|{}^{\cdots}_{\cdots}\rangle$ is zero, hence each state is a hyperfine singlet.

The T_d representation T_1 belonging to tableau $\{\mu\} = \{2,1,1\}$ is in reduced form with respect to the *threefold* axial invariance subgroup when represented in the tableau basis

$$\left\{ \begin{array}{|c|c|}\hline 1&2\\\hline 3\\\cline{1-1} 4\\\cline{1-1}\end{array} , \begin{array}{|c|c|}\hline 1&3\\\hline 2\\\cline{1-1} 4\\\cline{1-1}\end{array} , \begin{array}{|c|c|}\hline 1&4\\\hline 2\\\cline{1-1} 3\\\cline{1-1}\end{array} \right\} .$$

In Appendix B, it is transformed to the fourfold basis $\{[x],[y],[z]\}$. In this basis one finds

$$\mathfrak{D}^{[2,1,1]}[P^c] = \begin{array}{c} \begin{matrix} [x] & [y] & [z] \end{matrix} \\ \begin{pmatrix} 0 & 0 & 0 \\ 0 & 0 & 0 \\ 0 & 0 & 1 \end{pmatrix} \end{array} \quad (3.8)$$

for positive parity $[(-1)^p = 1]$ and a zero matrix results for negative parity. The conjugate spin states are a triplet $\{|{}^{\cdots}_{\cdots}\rangle, |{}^{\cdots}_{\cdots}\rangle, |{}^{\cdots}_{\cdots}\rangle\}$ of spin $(I=1)$, and so the only hyperfine triplet in the $O_4\downarrow O$ cluster consists of the positive parity states

$$\left|{}^{N^p}_{mn}[z]^{F^p}_{f}\right\rangle = \left|{}^{N^+}_{mn}\left[\frac{-2}{\sqrt{6}}\ \begin{array}{|c|c|}\hline 1&3\\\hline 2\\\cline{1-1} 4\\\cline{1-1}\end{array} + \frac{1}{\sqrt{3}}\ \begin{array}{|c|c|}\hline 1&4\\\hline 2\\\cline{1-1} 3\\\cline{1-1}\end{array}\right] F^p_f\right\rangle ,$$

where

$$F^p = (N+1)^+,\ N^+,\ \text{or}\ (N-1)^+ . \quad (3.9)$$

The representation T_2 belonging to tableau $\{3,1\}$

is spin-$\frac{1}{2}$ forbidden (tableaus such as $\left|\begin{matrix}\uparrow\uparrow\\ \downarrow\\ \uparrow\end{matrix}\right\rangle$ correspond to null states as explained in Sec. II B), and so the states (3.9) are inversion singlets. However, the T_1T_2 pair gives rise to inversion doublets in spin-1 molecules such as CD_4. (See Ref. 5, pp. 66 and 75 for examples of spin-1 levels.)

Finally, the representation A_2 belonging to tableau $\{1,1,1,1\}$ gives the following representation

$$\mathfrak{D}^{[1,1,1,1]}[P^c]=\begin{pmatrix}\boxed{1}\\ \boxed{2}\\ \boxed{3}\\ \boxed{4}\end{pmatrix}=(1) \tag{3.10}$$

for negative parity and a null result for positive parity. The conjugate tableau spin states are a quintet

$$\{|\uparrow\uparrow\uparrow\uparrow\rangle, |\uparrow\uparrow\uparrow\downarrow\rangle, |\uparrow\uparrow\downarrow\downarrow\rangle, |\uparrow\downarrow\downarrow\downarrow\rangle, |\downarrow\downarrow\downarrow\downarrow\rangle\}$$

of spin $(I=2)$, and so the only hyperfine quintet in the $O_4\dagger O$ cluster consists of negative parity states

$$\left|N^p\ mn\ \begin{matrix}\boxed{1}\\ \boxed{2}\\ \boxed{3}\\ \boxed{4}\end{matrix}\ F^p\ f\right\rangle=\left|N^-\ mn\ \begin{matrix}\boxed{1}\\ \boxed{2}\\ \boxed{3}\\ \boxed{4}\end{matrix}\ F^p=(N\pm2)^-,(N\pm1)^-,\text{ or } N^-\ f\right\rangle. \tag{3.11}$$

Once again, a "partner" representation, in this case it is $A_1=\boxed{1}\boxed{2}\boxed{3}\boxed{4}$, is spin-$\frac{1}{2}$ forbidden (it would take *spin* $\frac{9}{2}$ to activate the A_1), and so the states (3.11) are inversion singlets. Note that conventional labeling schemes[37] would name the three components of the $O_4\dagger O$ cluster as E, T_1, and A_1. We see that a more accurate labeling is $E^{\pm}$, T_1^+, and A_2^-, or better still, the unambiguous tableau labels in the preceding equations. (A comparison of tableau and standard symmetry labels is contained in Ref. 5.)

Now it is clear that the Hamiltonian representations in the $O_4\dagger O$ cluster basis will require diagonalization of just two 2×2 matrices formed between the two $F^p=N^+$ states (E^+ and T_1^+) and between the two $F^p=N^-$ states (E^- and A_2^-). Neither the pair of $F=N+1$ states nor the pair of $F=N-1$ states (T_1^+ and A_2^-) can interact via a Hamiltonian which has overall spatial inversion symmetry. (The parity changing effects of weak nuclear interactions are neglected here.) Consider the standard spin-rotation Hamiltonian[30] which has the form derived using (2.21), namely,

$$\begin{aligned}H_{sr}=&A\bar{N}_x[\bar{I}_z(1)+\bar{I}_z(2)+\bar{I}_z(3)+\bar{I}_z(4)]\\&+B\bar{N}_x[-\bar{I}_x(1)+\bar{I}_y(1)+\bar{I}_x(2)-\bar{I}_y(2)+\bar{I}_x(3)\\&+\bar{I}_y(3)-\bar{I}_x(4)-\bar{I}_y(4)]\end{aligned} \tag{3.12}$$

in the elementary cluster approximation in which one drops all $\bar{N}_x$ and $\bar{N}_y$ terms which connect different clusters. The matrix of this Hamiltonian in the Slater basis is shown below in (3.13) for the first 11 of the 16 states

$$\langle H_{psr}\rangle=\begin{array}{c|cccc|cccccc}
 & 1\bar{\uparrow} & 1\bar{\uparrow} & 1\bar{\uparrow} & 1\bar{\uparrow} & 1\bar{\downarrow} & 1\bar{\uparrow} & 1\bar{\uparrow} & 1\bar{\downarrow} & 1\bar{\uparrow} & 1\bar{\downarrow} & 1\bar{\downarrow}\\
 & 2\bar{\uparrow} & 2\bar{\uparrow} & 2\bar{\uparrow} & 2\bar{\downarrow} & 2\bar{\uparrow} & 2\bar{\uparrow} & 2\bar{\downarrow} & 2\bar{\uparrow} & 2\bar{\downarrow} & 2\bar{\uparrow} & 2\bar{\downarrow}\\
 & 3\bar{\uparrow} & 3\bar{\uparrow} & 3\bar{\downarrow} & 3\bar{\uparrow} & 3\bar{\uparrow} & 3\bar{\uparrow} & 3\bar{\uparrow} & 3\bar{\downarrow} & 3\bar{\downarrow} & 3\bar{\downarrow} & 3\bar{\downarrow}\\
 & 4\bar{\uparrow} & 4\bar{\downarrow} & 4\bar{\uparrow} & 4\bar{\uparrow} & 4\bar{\uparrow} & 4\bar{\downarrow} & 4\bar{\uparrow} & 4\bar{\uparrow} & 4\bar{\downarrow} & 4\bar{\uparrow} & 4\bar{\downarrow}\\
\hline
2a & -b\alpha_- & b\alpha_- & b\alpha_+ & -b\alpha_+ & & & & & & &\\
\hline
 & a & E & F & F & b\alpha_- & b\alpha_+ & -b\alpha_+ & 0 & 0 & 0\\
 & & a & F & F & -b\alpha_- & 0 & 0 & b\alpha_+ & -b\alpha_+ & 0\\
 & & & a & E & 0 & -b\alpha_- & 0 & b\alpha_- & 0 & -b\alpha_+\\
 & & & & a & 0 & 0 & -b\alpha_- & 0 & b\alpha_- & b\alpha_+\\
\hline
 & & & & & I & F & F & F & F & 0\\
 & & & & & & J & E & E & 0 & F\\
 & & & & & & & J & 0 & E & F\\
 & & & & & & & & J & E & F\\
 & & & & & & & & & J & F\\
 & & & & & & & & & & I
\end{array} \tag{3.13}$$

Here we let $a=nA$, $b=nB$, and $\alpha_\pm=\frac{1}{2}(1\pm i)=e^{\pm\pi i/4}/\sqrt{2}$. Also some pseudo-spin-spin exchange parameters I, J, E, and F are introduced. Spin-spin effects would be smaller than spin-rotation effects by a factor equal to the cluster momentum ($\langle\bar{N}_z\rangle=n\sim 10$–$100$) even if spin-spin and spin-rotation interaction constants were comparable. We include the spin-spin components to show the effects of differences in spin-exchange rates between nuclei across (E) and along (F) the rotation axis, as well as differences between energies of spins paired across (I) and along (J) this axis.

As in Sec. IID the next step is to use the assembly formula (Fig. 5) to arrive at the orbit spin basis. Tables III(a) and III(b) give the bases that are directly useful for threefold cluster calculations. To obtain useful fourfold states one must include the transformation from Appendix B for the $\{\mu\}=\{2,1,1\}$ tableau states. The results are listed in Tables IV(a) and IV(b). Finally the orbit spin matrices for even parity (3.14) and odd parity (3.15) states are obtained as in Sec. II

$$\langle H_{\rm psr}\rangle^+ = \begin{array}{|cccc|}\hline a & 0 & 0 & 0\\ & I+E-2F & 0 & 0\\ & 0 & J+E+2F & 0\\ & & & -a\\ \hline\end{array}\ , \qquad (3.14)$$

$$\langle H_{\rm psr}\rangle^- = \begin{array}{|cccccc|}\hline 2a & 0 & 0 & 0 & 0 & 0\\ & a & 0 & 0 & 0 & 0\\ & & I/3+2J/3 & \sqrt{2}(J-1 & 0 & \\ & & +\tfrac{4}{3}(E+2F) & +2E-2F)/3 & & 0\\ & & & 2I/3+J/3 & 0 & \\ & & & +2E/3-2F & & 0\\ & & & & -a & 0\\ & & & & & -2a\\ \hline\end{array}\ . \qquad (3.15)$$

Note that the tensor spin-rotation operator fails to give any off-diagonal matrix components whatsoever, i.e., the coefficient $b=Bn$ does not appear. Except for the presumably small pseudo-spin-spin coefficients the Hamiltonian is diagonal in the elementary ($O_4\uparrow O$) cluster basis. (However, real spin-spin interaction would give some additional off-diagonal components.)

To complete the problem one still needs to take account of the spin-frame transformation relations as was done in Secs. IIC and IID. The necessary coefficients are contained in Tables V and VI. As in the XY_3 example, one finds that only the diagonal components contribute significantly in the limit of high N and $n\sim N$. This is also the limit in which the tunneling parameter S and associated energy splittings

$$\begin{aligned}\langle E^\pm|H_{\rm cent}|E^\pm\rangle &= H^\pm+2S,\\ \langle T_1^+|H_{\rm cent}|T_1^+\rangle &= H^+,\\ \langle A_2^-|H_{\rm cent}|A_2^-\rangle &= H^- -4S\end{aligned} \qquad (3.16)$$

between cluster components become smaller than the hyperfine splittings determined by $a=An$, I, J, etc. This is case (2).

The limiting approach to case (2) is shown by the energy-level correlation diagram in Fig. 8. Here we choose E and F to be negligibly small but keep $I=-J=\frac{1}{4}a$. The resulting case (2) eigenvectors are most easily understood in terms of bracket tableau notation introduced at the end of Sec. IID, and are drawn next to their corresponding energy levels on the left-hand side of Fig. 8. In the case-(2) limit one may suppose that the permutations

TABLE III. Assembly formula applied to XY_4 spin states (a) $m_I=1$, (b) $m_I=0$. The three T_1 or $\{2,1,1\}$ states are in appropriate form for describing threefold cluster states. The others are appropriate for either type of clusters.

(a)	$\left\vert \begin{array}{|c|c\|}\hline 1&2\\\hline 3\\\cline{1-1} 4\\\cline{1-1}\end{array}, \begin{array}{|c|c|c\|}\hline \uparrow&\uparrow&\uparrow\\\hline \downarrow\\\cline{1-1}\end{array} \right\rangle$	$\left\vert \begin{array}{|c|c\|}\hline 1&3\\\hline 2\\\cline{1-1} 4\\\cline{1-1}\end{array}, \begin{array}{|c|c|c\|}\hline \uparrow&\uparrow&\uparrow\\\hline \downarrow\\\cline{1-1}\end{array} \right\rangle$	$\left\vert \begin{array}{|c|c\|}\hline 1&4\\\hline 2\\\cline{1-1} 3\\\cline{1-1}\end{array}, \begin{array}{|c|c|c\|}\hline \uparrow&\uparrow&\uparrow\\\hline \downarrow\\\cline{1-1}\end{array} \right\rangle$	$\left\vert \begin{array}{|c\|}\hline 1\\\hline 2\\\hline 3\\\hline 4\\\hline\end{array}, \begin{array}{|c|c|c|c\|}\hline \uparrow&\uparrow&\uparrow&\downarrow\\\hline\end{array} \right\rangle$
$1\uparrow 2\uparrow 3\uparrow 4\downarrow$	0	0	$\sqrt{3}/2$	1/2
$1\uparrow 2\uparrow 3\downarrow 4\uparrow$	0	$-2/\sqrt{6}$	$-1/2\sqrt{3}$	1/2
$1\uparrow 2\downarrow 3\uparrow 4\uparrow$	$1/\sqrt{2}$	$1/\sqrt{6}$	$-1/2\sqrt{3}$	1/2
$1\downarrow 2\uparrow 3\uparrow 4\uparrow$	$-1/\sqrt{2}$	$1/\sqrt{6}$	$-1/2\sqrt{3}$	1/2

(b)	$\left\vert \begin{array}{|c|c\|}\hline 1&2\\\hline 3&4\\\hline\end{array}, \begin{array}{|c|c|c\|}\hline \uparrow&\uparrow&\\\hline \downarrow&\downarrow&\\\hline\end{array} \right\rangle$	$\left\vert \begin{array}{|c|c\|}\hline 1&3\\\hline 2&4\\\hline\end{array}, \begin{array}{|c|c|c\|}\hline \uparrow&\uparrow&\\\hline \downarrow&\downarrow&\\\hline\end{array} \right\rangle$	$\left\vert \begin{array}{|c|c\|}\hline 1&2\\\hline 3\\\cline{1-1} 4\\\cline{1-1}\end{array}, \begin{array}{|c|c|c\|}\hline \uparrow&\uparrow&\uparrow\\\hline \downarrow\\\cline{1-1}\end{array} \right\rangle$	$\left\vert \begin{array}{|c|c\|}\hline 1&3\\\hline 2\\\cline{1-1} 4\\\cline{1-1}\end{array}, \begin{array}{|c|c|c\|}\hline \uparrow&\uparrow&\downarrow\\\hline \downarrow\\\cline{1-1}\end{array} \right\rangle$	$\left\vert \begin{array}{|c|c\|}\hline 1&4\\\hline 2\\\cline{1-1} 3\\\cline{1-1}\end{array}, \begin{array}{|c|c|c\|}\hline \uparrow&\uparrow&\downarrow\\\hline \downarrow\\\cline{1-1}\end{array} \right\rangle$	$\left\vert \begin{array}{|c\|}\hline 1\\\hline 2\\\hline 3\\\hline 4\\\hline\end{array}, \begin{array}{|c|c|c|c\|}\hline \uparrow&\uparrow&\downarrow&\downarrow\\\hline\end{array} \right\rangle$
$1\uparrow 2\uparrow 3\downarrow 4\downarrow$	0	$-1/\sqrt{3}$	0	$-1/\sqrt{3}$	$1/\sqrt{6}$	$1/\sqrt{6}$
$1\uparrow 2\downarrow 3\uparrow 4\downarrow$	1/2	$1/2\sqrt{3}$	1/2	$1/2\sqrt{3}$	$1/\sqrt{6}$	$1/\sqrt{6}$
$1\downarrow 2\uparrow 3\uparrow 4\downarrow$	−1/2	$1/2\sqrt{3}$	−1/2	$1/2\sqrt{3}$	$1/\sqrt{6}$	$1/\sqrt{6}$
$1\uparrow 2\downarrow 3\downarrow 4\uparrow$	−1/2	$1/2\sqrt{3}$	1/2	$-1/2\sqrt{3}$	$-1/\sqrt{6}$	$1/\sqrt{6}$

TABLE III. *(Continued)*.

(b)										
	$\begin{array}{\|c\|c\|}\hline 1&2\\\hline 3&4\\\hline\end{array}$, $\begin{array}{\|c\|}\hline\uparrow\\\hline\uparrow\\\hline\uparrow\\\hline\uparrow\\\hline\end{array}$	$\begin{array}{\|c\|c\|}\hline 1&3\\\hline 2&4\\\hline\end{array}$, $\begin{array}{\|c\|c\|}\hline\uparrow&\uparrow\\\hline\uparrow&\uparrow\\\hline\end{array}$	$\begin{array}{\|c\|c\|c\|}\hline 1&2&\\\hline 3&4&\\\hline\end{array}$, $\begin{array}{\|c\|c\|}\hline\uparrow&\uparrow\\\hline\uparrow&\\\hline\end{array}$	$\begin{array}{\|c\|c\|c\|}\hline 1&3&\\\hline 2&4&\\\hline\end{array}$, $\begin{array}{\|c\|c\|}\hline\uparrow&\uparrow\\\hline\uparrow&\\\hline\end{array}$	$\begin{array}{\|c\|c\|c\|}\hline 1&4&\\\hline 2&3&\\\hline\end{array}$, $\begin{array}{\|c\|c\|}\hline\uparrow&\uparrow\\\hline\uparrow&\\\hline\end{array}$	$\begin{array}{\|c\|c\|}\hline 1&2\\\hline 3&4\\\hline\end{array}$, $\begin{array}{\|c\|c\|}\hline\uparrow&\uparrow\\\hline\uparrow&\uparrow\\\hline\end{array}$				
$\begin{array}{\|c\|c\|c\|c\|}\hline 1\uparrow&2\uparrow&3\uparrow&4\uparrow\\\hline\end{array}$	1/2	$1/2\sqrt{3}$	−1/2	$-1/2\sqrt{3}$	$-1/\sqrt{6}$	$1/\sqrt{6}$				
$\begin{array}{\|c\|c\|c\|c\|}\hline 1\downarrow&2\uparrow&3\uparrow&4\uparrow\\\hline\end{array}$	0	$-1/\sqrt{3}$	0	$1/\sqrt{3}$	$-1/\sqrt{6}$	$1/\sqrt{6}$				

between nuclei in "bottom" states (1 and 2) and those in "top" states (3 and 4) are no longer feasible, i.e., XY_4 has become a pair of diatomic X_2 molecules as far as permutations are concerned.

By expressing the eigenvectors of (3.14) and (3.15) in terms of partially symmetrized or broken tableau one obtains (3.17)–(3.19) below using Tables III, IV, and Eq. (2.13). The first three states cannot mix with any others in the cluster.

$$\left|\begin{array}{|c|}\hline 1\\\hline 2\\\hline 3\\\hline 4\\\hline\end{array}\ \uparrow\uparrow\uparrow\uparrow\right\rangle = \left|\begin{array}{|c|c|}\hline 1&2\\\hline\end{array}\ \uparrow\uparrow\right\rangle\left|\begin{array}{|c|c|}\hline 3&4\\\hline\end{array}\ \uparrow\uparrow\right\rangle, \tag{3.17a}$$

$$\left|\begin{array}{|c|}\hline 1\\\hline 2\\\hline 3\\\hline 4\\\hline\end{array}\ \uparrow\uparrow\uparrow\downarrow\right\rangle = \left[\left|\begin{array}{|c|c|}\hline 1&2\\\hline\end{array}\ \uparrow\uparrow\right\rangle\left|\begin{array}{|c|c|}\hline 3&4\\\hline\end{array}\ \uparrow\downarrow\right\rangle + \left|\begin{array}{|c|c|}\hline 1&2\\\hline\end{array}\ \uparrow\downarrow\right\rangle\left|\begin{array}{|c|c|}\hline 3&4\\\hline\end{array}\ \uparrow\uparrow\right\rangle\right]/\sqrt{2}, \tag{3.17b}$$

$$\left|\begin{array}{|c|c|}\hline z&\\\hline\uparrow&\\\hline\downarrow&\\\hline\end{array}\ \uparrow\uparrow\right\rangle = \left[\left|\begin{array}{|c|c|}\hline 1&2\\\hline\end{array}\ \uparrow\uparrow\right\rangle\left|\begin{array}{|c|c|}\hline 3&4\\\hline\end{array}\ \uparrow\downarrow\right\rangle - \left|\begin{array}{|c|c|}\hline 1&2\\\hline\end{array}\ \uparrow\downarrow\right\rangle\left|\begin{array}{|c|c|}\hline 3&4\\\hline\end{array}\ \uparrow\uparrow\right\rangle\right]/\sqrt{2}. \tag{3.17c}$$

The form of the next four eigenstates depends on spin Hamiltonian, however. For our choice we have

$$\left|\begin{array}{|c|c|}\hline 1&2\\\hline 3&4\\\hline\end{array}\ \begin{array}{c}\uparrow\uparrow\\\downarrow\downarrow\end{array}\right\rangle = \left|\begin{array}{|c|c|}\hline 1&2\\\hline\end{array}\ \begin{array}{c}\uparrow\\\downarrow\end{array}\right\rangle\left|\begin{array}{|c|c|}\hline 3&4\\\hline\end{array}\ \begin{array}{c}\uparrow\\\downarrow\end{array}\right\rangle, \tag{3.18a}$$

$$\frac{2}{\sqrt{6}}\left|\begin{array}{|c|c|}\hline 1&3\\\hline 2&4\\\hline\end{array}\ \begin{array}{c}\uparrow\uparrow\\\downarrow\downarrow\end{array}\right\rangle + \frac{1}{\sqrt{3}}\left|\begin{array}{|c|}\hline 1\\\hline 2\\\hline 3\\\hline 4\\\hline\end{array}\ \uparrow\uparrow\uparrow\downarrow\right\rangle = \left|\begin{array}{|c|c|}\hline 1&2\\\hline\end{array}\ \uparrow\downarrow\right\rangle\left|\begin{array}{|c|c|}\hline 3&4\\\hline\end{array}\ \uparrow\downarrow\right\rangle \tag{3.18b}$$

of energy J, and

$$\left|\begin{array}{|c|c|}\hline z&\\\hline\downarrow&\\\hline\uparrow&\\\hline\end{array}\ \uparrow\uparrow\uparrow\right\rangle = \left[\left|\begin{array}{|c|c|}\hline 1&2\\\hline\end{array}\ \uparrow\uparrow\right\rangle\left|\begin{array}{|c|c|}\hline 3&4\\\hline\end{array}\ \downarrow\downarrow\right\rangle - \left|\begin{array}{|c|c|}\hline 1&2\\\hline\end{array}\ \downarrow\downarrow\right\rangle\left|\begin{array}{|c|c|}\hline 3&4\\\hline\end{array}\ \uparrow\uparrow\right\rangle\right]/\sqrt{2}, \tag{3.19a}$$

$$\frac{-1}{\sqrt{3}}\left|\begin{array}{|c|c|}\hline 1&3\\\hline 2&4\\\hline\end{array}\ \begin{array}{c}\uparrow\uparrow\\\downarrow\downarrow\end{array}\right\rangle + \frac{2}{\sqrt{6}}\left|\begin{array}{|c|}\hline 1\\\hline 2\\\hline 3\\\hline 4\\\hline\end{array}\ \uparrow\uparrow\downarrow\downarrow\right\rangle = \left[\left|\begin{array}{|c|c|}\hline 1&2\\\hline\end{array}\ \uparrow\uparrow\right\rangle\left|\begin{array}{|c|c|}\hline 3&4\\\hline\end{array}\ \downarrow\downarrow\right\rangle + \left|\begin{array}{|c|c|}\hline 1&2\\\hline\end{array}\ \downarrow\downarrow\right\rangle\left|\begin{array}{|c|c|}\hline 3&4\\\hline\end{array}\ \uparrow\uparrow\right\rangle\right]/\sqrt{2} \tag{3.19b}$$

TABLE IV. $(T_1, \{2,1,1\})$ states transformed to appropriate fourfold cluster form. The transformation (B1) was applied to the $\{2,1,1\}$ states in Table II.

(a)	$\lvert x, \uparrow\uparrow\uparrow\downarrow \rangle$	$\lvert y, \uparrow\uparrow\uparrow\downarrow \rangle$	$\lvert z, \uparrow\uparrow\uparrow\downarrow \rangle$
$1\uparrow 2\uparrow 3\uparrow 4\downarrow$	1/2	1/2	1/2
$1\uparrow 2\uparrow 3\downarrow 4\uparrow$	−1/2	−1/2	1/2
$1\uparrow 2\downarrow 3\uparrow 4\uparrow$	1/2	−1/2	−1/2
$1\downarrow 2\uparrow 3\uparrow 4\uparrow$	−1/2	1/2	−1/2

(b)	$\lvert x, \uparrow\uparrow\uparrow\downarrow \rangle$	$\lvert y, \uparrow\uparrow\uparrow\downarrow \rangle$	$\lvert z, \uparrow\uparrow\uparrow\downarrow \rangle$
$1\uparrow 2\uparrow 3\downarrow 4\downarrow$	0	0	$1/\sqrt{2}$
$1\uparrow 2\downarrow 3\uparrow 4\downarrow$	$1/\sqrt{2}$	0	0
$1\downarrow 2\uparrow 3\uparrow 4\downarrow$	0	$1/\sqrt{2}$	0
$1\uparrow 2\downarrow 3\downarrow 4\uparrow$	0	$-1/\sqrt{2}$	0
$1\downarrow 2\uparrow 3\downarrow 4\uparrow$	$-1/\sqrt{2}$	0	0
$1\downarrow 2\downarrow 3\uparrow 4\uparrow$	0	0	$-1/\sqrt{2}$

TABLE V. Spin frame relations for angular momentum $I=1$.

$\langle N\ n\ F\ f \rangle$	$\left\vert \begin{array}{c}\square\square \\ \square \end{array} \uparrow\uparrow\uparrow \right\rangle$	$\left\vert \begin{array}{c}\square\square \\ \square \end{array} \uparrow\uparrow\downarrow \right\rangle$	$\left\vert \begin{array}{c}\square\square \\ \square \end{array} \uparrow\downarrow\downarrow \right\rangle$
$\langle N\ n\ F=N+1\ f\vert$	$\left(\frac{(N+n+1)(N+n+2)}{(2N+2)(2N+3)}\right)^{1/2}$	$\left(\frac{2(N+n+1)(N-n+1)}{(2N+2)(2N+3)}\right)^{1/2}$	$\left(\frac{(N-n+1)(N-n+2)}{(2N+2)(2N+3)}\right)^{1/2}$
$\langle F=N\vert$	$\left(\frac{(N-n)(N+n+1)}{N(2N+2)}\right)^{1/2}$	$-\left(\frac{2n^2}{N(2N+2)}\right)^{1/2}$	$-\left(\frac{(N+n)(N-n+1)}{N(2N+2)}\right)^{1/2}$
$\langle F=N-1\vert$	$\left(\frac{(N-n-1)(N-n)}{2N(2N-1)}\right)^{1/2}$	$-\left(\frac{2(N+n)(N-n)}{2N(2N-1)}\right)^{1/2}$	$\left(\frac{(N+n-1)(N+n)}{2N(2N-1)}\right)^{1/2}$

of energy I. The remaining three states are just the down-spin images of (3.17).

In Fig. 8 we assume that inversion splitting is zero, i.e., that $H^{+}=H^{-}$ in (3.16). This is equivalent to prohibiting the nuclear masses from performing an odd permutation such as (ab). Nevertheless, we note that the

$$\left(\begin{array}{|c|c|}\hline 1&2\\\hline 3&4\\\hline\end{array}\ ,\ \begin{array}{|c|c|}\hline 1&3\\\hline 2&4\\\hline\end{array} \right)$$

inversion doublet is split by hyperfine spin-spin splitting is $(\frac{4}{3}J-\frac{2}{3}I+\frac{1}{3}E+4F)$. Furthermore, if the spin exchange E and F are nonzero the degeneracy between positive and negative parity doublets in extreme case (2) on the left-hand side of Fig. 8 will be lifted. In other words, the exchange of either nuclear-spin states or the nuclei themselves will split "inversion doublets."

APPENDIX A: IRREDUCIBLE REPRESENTATIONS AND PROJECTION OPERATORS OF PERMUTATION GROUPS S_n

The representations of the order-2 permutation group $S_2=[1=(a)(b),(ab)]$ given by (A1) below are well known,

$$\mathfrak{D}^{\{2\}}[(a)(b)]=\left\vert \begin{array}{|c|c|}\hline a&b\\\hline\end{array}\right\rangle = (1),\quad \mathfrak{D}^{\{1,1\}}[(a)(b)]=\left\vert \begin{array}{|c|}\hline a\\\hline b\\\hline\end{array}\right\rangle = (1),\qquad \text{(A1)}$$

$$\mathfrak{D}^{\{2\}}[(ab)]=(1),\quad \mathfrak{D}^{\{1,1\}}[(ab)]=(-1)$$

though the tableau notation is seldom emphasized. The horizontal (vertical) tableaus correspond to symmetrizing (antisymmetrizing) projection operators

$$P^{\{2\}}=\tfrac{1}{2}[1+(ab)],\quad P^{\{1,1\}}=\tfrac{1}{2}[1-(ab)]. \qquad \text{(A2)}$$

However, for more complicated permutation groups, starting with

$$S_3=\{1=(a)(b)(c),(ab),(bc),(ac),(abc),(acb)\}$$

the power and convenience of the tableau coding should not be overlooked. First, the tableaus are arranged so that if you delete the most recently added particle [for S_3 it is (c)] the resulting subtableaus indicate the subgroup representations on the diagonal as in the following:

$$\mathfrak{D}^{\{3\}}[1]=\left\vert \begin{array}{|c|c|c|}\hline a&b&c\\\hline\end{array}\right\rangle = (1),$$

$$\mathfrak{D}^{\{2,1\}}[1]=\begin{pmatrix}\left\vert \begin{array}{|c|c|}\hline a&b\\\hline c\\\cline{1-1}\end{array}\right\rangle & 0\\ 0 & \left\vert \begin{array}{|c|c|}\hline a&c\\\hline b\\\cline{1-1}\end{array}\right\rangle\end{pmatrix} = \begin{pmatrix}1&0\\0&1\end{pmatrix},$$

$$\mathfrak{D}^{\{1,1,1\}}[1]=\left\vert \begin{array}{|c|}\hline a\\\hline b\\\hline c\\\hline\end{array}\right\rangle = (1)\ ; \qquad \text{(A3a)}$$

$$\mathfrak{D}^{\{3\}}[(ab)]=(1),$$

$$\mathfrak{D}^{\{2,1\}}[(ab)]=\begin{pmatrix}1&0\\0&-1\end{pmatrix},$$

$$\mathfrak{D}^{\{1,1,1\}}[(ab)]=(-1). \qquad \text{(A3b)}$$

[Note the

$$\begin{array}{|c|}\hline a\\\hline b\\\hline\end{array}\ \text{in}\ \begin{array}{|c|c|}\hline a&c\\\hline b\\\cline{1-1}\end{array}\ \text{and}\ \begin{array}{|c|}\hline a\\\hline b\\\hline c\\\hline\end{array}$$

which gives the (-1) in each case for S_2 permutation (ab).] Second, the Yamanouchi tableau formula given in Fig. 9 and explained in the caption allows one to quickly compute the representation of the permutation involving the two most recently added particles [for S_3 it is (bc)] and hence all

TABLE VI. Spin frame relations for angular momentum $I=2$. For typographical and computer coding simplicity the following notation is used: $(X+a:b)=(X+a)(X+a+1)\ldots(X+b)$, where

$U=N+n$, $W_2=2N+2:5$, $W_1=2N(2N+2:4)$, $V=N-n$, $W_{-2}=2N-3:0$, $W_{-1}=(2N+2)(2N-2:0)$, and $W_0=(2N-1:0)(2N+2:3)$.

$\langle$ 1 2 / 3 4 $\rangle$	$\left\vert \begin{array}{|c|c|}\hline 1&2\\\hline 3&4\\\hline\end{array} \right\rangle$	$\left\vert \begin{array}{|c|c|c|}\hline 1&2&3\\\hline 4\\\cline{1-1}\end{array} \right\rangle$	$\left\vert \begin{array}{|c|c|c|c|}\hline 1&2&3&4\\\hline\end{array} \right\rangle$
$\langle N \; F=N+2 \mid n \; f \rangle$	$\left(\frac{U+1:4}{W_2}\right)^{1/2}$	$2\left(\frac{(U+1:3)(V+1)}{W_2}\right)^{1/2}$	$\left(\frac{6(U+1:2)(V+1:2)}{W_2}\right)^{1/2}$	$2\left(\frac{(U+1)(V+1:3)}{W_2}\right)^{1/2}$	$\left(\frac{V+1:4}{W_2}\right)^{1/2}$
$\langle F=N+1 \mid$	$2\left(\frac{(U+1:3)V}{W_1}\right)^{1/2}$	$2(N-2n)\left(\frac{U+1:2}{W_1}\right)^{1/2}$	$-2n\left(\frac{6(U+1)(V+1)}{W_1}\right)^{1/2}$	$-2(N+2n)\left(\frac{V+1:2}{W_1}\right)^{1/2}$	$-2\left(\frac{U(V+1:3)}{W_1}\right)^{1/2}$
$\langle F=N \mid$	$\left(\frac{6(U+0:2)(V-1)}{W_0}\right)^{1/2}$	$-(2n+1)\left(\frac{6(U+1)V}{W_0}\right)^{1/2}$	$\left(\frac{2[3n^2-N(N+1)]}{W_0}\right)^{1/2}$	$(2n-1)\left(\frac{6U(V+1)}{W_0}\right)^{1/2}$	$\left(\frac{6(U-1)(V+0:2)}{W_0}\right)^{1/2}$
$\langle F=N-1 \mid$	$2\left(\frac{(U+1)(V-2:0)}{W_{-1}}\right)^{1/2}$	$-2(N+2n+1)\left(\frac{V-1:0}{W_{-1}}\right)^{1/2}$	$2n\left(\frac{6UV}{W_{-1}}\right)^{1/2}$	$2(N-2n+1)\left(\frac{U-1:0}{W_{-1}}\right)^{1/2}$	$-2\left(\frac{(U-2:0)(V+1)}{W_{-1}}\right)^{1/2}$
$\langle F=N-2 \mid$	$\left(\frac{V-3:0}{W_{-2}}\right)^{1/2}$	$-2\left(\frac{U(V-2:0)}{W_{-2}}\right)^{1/2}$	$\left(\frac{6(U-1:0)(V-1:0)}{W_{-2}}\right)^{1/2}$	$-2\left(\frac{(U-2:0)V}{W_{-2}}\right)^{1/2}$	$\left(\frac{U-3:0}{W_{-2}}\right)^{1/2}$

other permutations as well. For S_3, Fig. 9 gives

$$\mathfrak{D}^{\{3\}}[(bc)]=\left|\begin{array}{|c|c|c|}\hline a&b&c\\\hline\end{array}\right\rangle_{(1)},$$

$$\mathfrak{D}^{\{2,1\}}[(bc)]=\begin{pmatrix}\left|\begin{array}{|c|c|}\hline a&b\\\hline c\\\cline{1-1}\end{array}\right\rangle_{-\frac{1}{2}} & \left|\begin{array}{|c|c|}\hline a&c\\\hline b\\\cline{1-1}\end{array}\right\rangle_{\frac{1}{2}\sqrt{3}} \\ {\scriptstyle\frac{1}{2}\sqrt{3}} & {\scriptstyle\frac{1}{2}}\end{pmatrix},$$

$$\mathfrak{D}^{\{1,1,1\}}[(bc)]=\left|\begin{array}{|c|}\hline a\\\hline b\\\hline c\\\hline\end{array}\right\rangle_{(-1)} \tag{A3c}$$

and matrix multiplication [viz., $(ac)=(ab)(bc)(ab)$, $(abc)=(ab)(ac)$, and $(acb)=(ac)(ab)$] gives the rest:

$$\mathfrak{D}^{\{3\}}[(ac)]=(1),$$

$$\mathfrak{D}^{\{2,1\}}[(ac)]=\begin{pmatrix}-\frac{1}{2} & -\frac{1}{2}\sqrt{3}\\ -\frac{1}{2}\sqrt{3} & \frac{1}{2}\end{pmatrix},$$

$$\mathfrak{D}^{\{1,1,1\}}[(bc)]=(-1); \tag{A3d}$$

$$\mathfrak{D}^{\{3\}}[(abc)]=(1),$$

$$\mathfrak{D}^{\{2,1\}}[(abc)]=\begin{pmatrix}-\frac{1}{2} & -\frac{1}{2}\sqrt{3}\\ \frac{1}{2}\sqrt{3} & -\frac{1}{2}\end{pmatrix},$$

$$\mathfrak{D}^{\{1,1,1\}}[(abc)]=(1); \tag{A3e}$$

$$\mathfrak{D}^{\{3\}}[(acb)]=(1),$$

$$\mathfrak{D}^{\{2,1\}}[(acb)]=\begin{pmatrix}-\frac{1}{2} & \frac{1}{2}\sqrt{3}\\ -\frac{1}{2}\sqrt{3} & -\frac{1}{2}\end{pmatrix},$$

$$\mathfrak{D}^{\{1,1,1\}}[(acb)]=(1). \tag{A3f}$$

The projection operators are given by

$$P^{\{\mu\}}_{\{i\}\{j\}}=\frac{l^{\{\mu\}}}{n!}\sum_{(p)}\mathfrak{D}^{\{\mu\}*}_{\{i\}\{j\}}[(p)](p), \tag{A4}$$

where $l^{\{\mu\}}$ is the dimension of $\mathfrak{D}^{\{\mu\}}$. For example, combining (A3) and (A4), we have

$$P^{\{2,1\}}_{\begin{array}{|c|c|}\hline a&b\\\hline c\\\cline{1-1}\end{array}\;\begin{array}{|c|c|}\hline a&b\\\hline c\\\cline{1-1}\end{array}}=2/3![2(1)-(ac)-(abc)+2(ab)-(acb)-(bc)]/2, \tag{A5}$$

$$P^{\{2,1\}}_{\begin{array}{|c|c|}\hline a&c\\\hline b\\\cline{1-1}\end{array}\;\begin{array}{|c|c|}\hline a&b\\\hline c\\\cline{1-1}\end{array}}=2/3![-(ac)+(abc)-(acb)+(bc)]\sqrt{3}/2,$$

which are used in Fig. 3.

Some examples of

$$S_4=\{1,\bar{r}_1=(abc),I\bar{i}_3=(cd),I\bar{R}_3=(acbd),\ldots\}$$

representations which are used in Sec. III are given below.

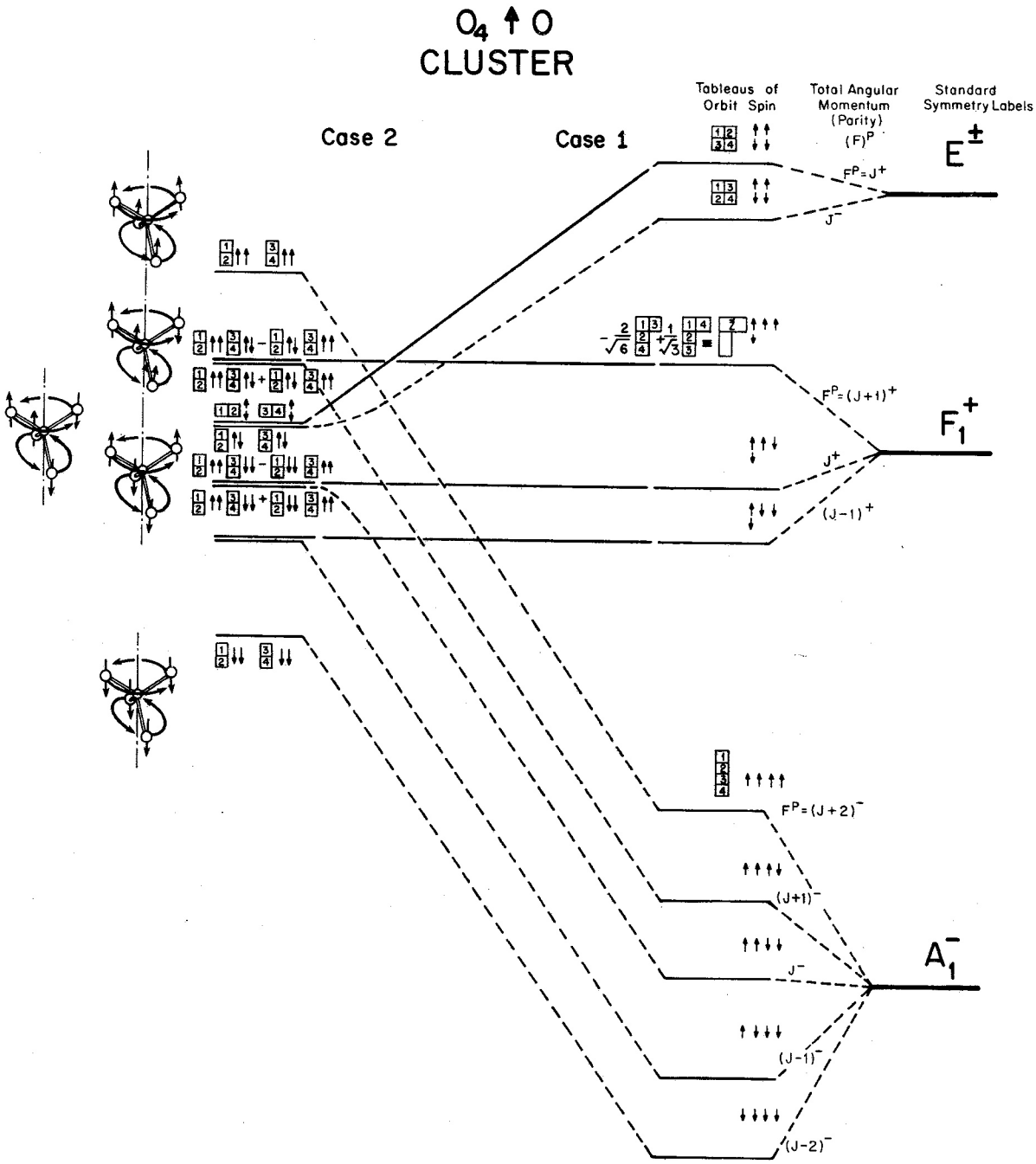

FIG. 8. XY_4 superhyperfine correlation between cases (1) and (2) for $(O_4)+O$ cluster. Energy levels obtained from (3.14)–(3.16) are plotted as a function of the cluster tunneling parameter (S) for fixed spin-rotation parameter a and fixed pseudo-spin-spin parameters $I=-J=\frac{1}{4}a$, $E=0=F$. Real inversion splitting is assumed zero ($H^+=H^-$).

$[p]$	$\mathfrak{D}^{\{2,2\}}_{[p]}=$	$\mathfrak{D}^{\{2,1,1\}}_{[p]}=$	$\mathfrak{D}^{\{1,1,1,1\}}_{[p]}=$	
	$\left\vert \begin{array}{|c|c|}\hline a & b \\ \hline c & d \\ \hline \end{array} \right\rangle \left\vert \begin{array}{|c|c|}\hline a & c \\ \hline b & d \\ \hline \end{array} \right\rangle$	$\left\vert \begin{array}{|c|c|}\hline a & b \\ \hline c \\ \cline{1-1} d \\ \cline{1-1} \end{array} \right\rangle \left\vert \begin{array}{|c|c|}\hline a & c \\ \hline b \\ \cline{1-1} d \\ \cline{1-1} \end{array} \right\rangle \left\vert \begin{array}{|c|c|}\hline a & d \\ \hline b \\ \cline{1-1} c \\ \cline{1-1} \end{array} \right\rangle$	$\left\vert \begin{array}{|c|}\hline a \\ \hline b \\ \hline c \\ \hline d \\ \hline \end{array} \right\rangle$	
$[1]$	$\begin{pmatrix} 1 & 0 \\ 0 & 1 \end{pmatrix}$	$\begin{pmatrix} 1 & 0 & 0 \\ 0 & 1 & 0 \\ 0 & 0 & 1 \end{pmatrix}$	(1)	(A6a)
$[(abc)]$	$\begin{pmatrix} -1/2 & -\sqrt{3}/2 \\ \sqrt{3}/2 & -1/2 \end{pmatrix}$	$\begin{pmatrix} -1/2 & -\sqrt{3}/2 & 0 \\ \sqrt{3}/2 & -1/2 & 0 \\ 0 & 0 & 1 \end{pmatrix}$	(1)	(A6b)
$[(acbd)]$	$\begin{pmatrix} 1 & 0 \\ 0 & -1 \end{pmatrix}$	$\begin{pmatrix} 0 & -\sqrt{3}/3 & -\sqrt{6}/3 \\ \sqrt{3}/3 & 2/3 & -\sqrt{2}/3 \\ \sqrt{6}/3 & -\sqrt{2}/3 & 1/3 \end{pmatrix}$	(-1)	(A6c)

Note S_3 irreducible representation bases

$\begin{array}{|c|c|}\hline a & b \\ \hline c \\ \cline{1-1} \end{array}$, $\begin{array}{|c|c|}\hline a & c \\ \hline b \\ \cline{1-1} \end{array}$, and $\begin{array}{|c|}\hline a \\ \hline b \\ \hline c \\ \hline \end{array}$

"inside" the $\{2,1,1\}$ tableaus locate these representations in reduced block diagonal form in (A6a) and (A6b).

APPENDIX B: THREEFOLD-TO-FOURFOLD TRANSFORMATIONS

The structure of the tableaus guarantees that S_4 representations are already in block diagonalized reduced form with respect to $S_3=\{1,(ab),(bc),\ldots\}$ as well as $S_2=\{1,(ab)\}$. Physically, this means that the $T_d \sim S_4$ representations are already in reduced form with respect to a threefold axial subgroup $C_{3v} \sim S_3=\{1,\sigma,\sigma',\ldots\}$.

For applications in Sec. III we need representations that are reduced with respect to the fourfold axial subgroup

$$D_{2d}=\{1,I\bar{R}_3,\bar{R}_3^2,I\bar{R}_3^3,R_1^2,R_2^2,Ii_3,Ii_4\}$$
$$=\{1,(acbd),(ab)(cd),(adbc),(ac)(bd),$$
$$(ad)(bc),(cd),(ab)\}.$$

Clearly from (A6c) the representation $\mathfrak{D}^{\{2,1,1\}}$ is not in this form, although $\mathfrak{D}^{\{2,2\}}$ and $\mathfrak{D}^{\{1,1,1,1\}}$ are. (For $\mathfrak{D}^{\{1,1,1,1\}}$ or $\mathfrak{D}^{\{4\}}$ this is trivially so.) However, the following orthogonal transformation produces bases which are in D_{2d} reduced form:

$$\left\vert \begin{array}{|c|c|}\hline x & \\ \hline & \\ \cline{1-1} \end{array} \right\rangle = \frac{1}{\sqrt{2}} \left\vert \begin{array}{|c|c|}\hline a & b \\ \hline c \\ \cline{1-1} d \\ \cline{1-1} \end{array} \right\rangle + \frac{1}{\sqrt{6}} \left\vert \begin{array}{|c|c|}\hline a & c \\ \hline b \\ \cline{1-1} d \\ \cline{1-1} \end{array} \right\rangle + \frac{1}{\sqrt{3}} \left\vert \begin{array}{|c|c|}\hline a & d \\ \hline b \\ \cline{1-1} c \\ \cline{1-1} \end{array} \right\rangle, \qquad \text{(B1a)}$$

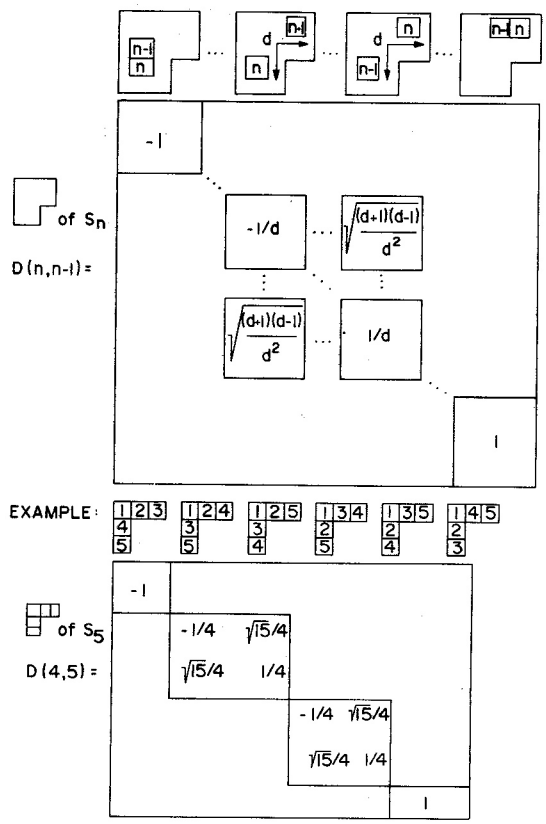

FIG. 9. Yamanouchi formulas for permutation operators. Integer d is the "city block" distance between n and $n-1$ blocks, i.e., the minimum number of streets to be crossed when traveling from one to the other. Note that when numbers n and $n-1$ are ordered smaller above larger, the permutation is negative (antisymmetric if $d=1$), and positive (symmetric if $d=1$) when the smaller number is left of the larger number. (The $n-1$ will never be above *and* left of n since that arrangement would be "nonlexical.")

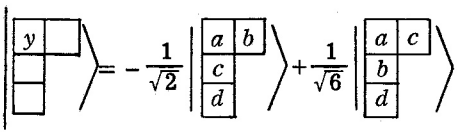

$$+\frac{1}{\sqrt{3}}\left|\begin{array}{|c|c|}\hline a & d\\\hline b\\\cline{1-1} c\\\cline{1-1}\end{array}\right\rangle, \qquad \text{(B1b)}$$

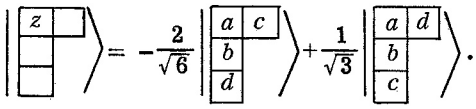

Examples of the resulting representation are the following:

$$\mathfrak{D}^{T1}[\bar{r}_1 \text{ or } (abc)] = \begin{array}{c} \\ \langle[x]| \\ \langle[y]| \\ \langle[z]| \end{array} \begin{array}{c} \begin{array}{ccc} |[x]\rangle & |[y]\rangle & |[z]\rangle \end{array} \\ \begin{pmatrix} 0 & 0 & 1 \\ 1 & 0 & 0 \\ 0 & 1 & 0 \end{pmatrix} \end{array},$$

$$\mathfrak{D}^{T1}[I\bar{R}_3 \text{ or } (acbd)] = \begin{array}{c} \\ \langle[x]| \\ \langle[y]| \\ \langle[z]| \end{array} \begin{array}{c} \begin{array}{ccc} |[x]\rangle & |[y]\rangle & |[z]\rangle \end{array} \\ \begin{pmatrix} 0 & -1 & 0 \\ 1 & 0 & 0 \\ 0 & 0 & 1 \end{pmatrix} \end{array} \qquad \text{(B2)}$$

and these are just the well-known cubic polar-vector or tetrahedral axial-vector representations.

*Present address: School of Physics, Georgia Institute of Technology, Atlanta, GA, 30332.

[1]K. Fox, H. W. Galbraith, B. J.Krohn, and J. D. Louck, Phys. Rev. A 15, 1363 (1977).

[2]R. S. McDowell, in *Laser Spectroscopy III*, edited by J. L. Hall and J. L. Carlsten (Springer-Verlag, New York, 1977), p. 102.

[3]W. G. Harter and C. W. Patterson, Phys. Rev. Lett. 38, 224 (1977); J. Chem. Phys. 66, 4872 (1977); Int. J. Quantum Chem. Symp. No. 11, 479 (1977).

[4]C. W. Patterson and W. G. Harter, J. Chem. Phys. 66, 4886 (1977).

[5]W. G. Harter, C. W. Patterson, and F. J. daPaixao, Rev. Mod. Phys. 50, 37 (1978).

[6]H. P. Layer and S. R. Peterson (private communication); W. G. Harter, H. P. Layer, and S. R. Peterson, Opt. Lett. 4, 90 (1979).

[7]A. S. Pine, J. Opt. Soc. Am. 66, 97 (1976).

[8]P. Rabinowitz (private communication).

[9]M. Loete, A. Claron, A. Fricket, R. S. McDowell, H. W. Galbraith, J. C. Hillico, J. Moret-Bailly, and L. Henry, C. R. Acad. Sci. B (Paris) 158 (1977).

[10]A. J. Dorney and J. K. G. Watson, J. Mol. Spectrosc. 42, 135 (1972).

[11]J. K. G. Watson, in 32nd Molecular Spectroscopy Symposium, Ohio State University, 1977 (unpublished), abstract WA1.

[12]B. J. Krohn, Los Alamos Report No. LA-6554-MS, 1976 (unpublished).

[13]J. L. Hall and C. L. Bordé, Phys. Rev. Lett. 30, 1101 (1973).

[14]J. Bordé, M. Ouhayoun, and C. J. Bordé, in 33rd Molecular Spectroscopy Symposium, Ohio State University, 1978 (unpublished), abstract FA4.

[15]W. G. Harter and C. W. Patterson, *Advances in Laser Chemistry*, edited by A. H. Zewail (Springer-Verlag, New York, 1978).

[16]H. W. Galbraith, C. W. Patterson, B. J. Krohn, and W. G. Harter, J. Mol. Spectrosc. 73, 475 (1978).

[17]U. Fano, Phys. Rev. A 2, 353 (1970); E. S. Chang and U. Fano, *ibid.* 6, 173 (1972).

[18]D. E. Rutherford, *Substitutional Analysis* (Edinburgh University, Edinburgh, 1947).

[19]H. Weyl, *Theory of Groups and Quantum Mechanics* (Dover, New York, 1931).

[20]W. A. Goddard, III, Phys. Rev. 157, 73 (1967).

[21]W. G. Harter, Phys. Rev. A 8, 2819 (1973).

[22]W. G. Harter and C. W. Patterson, Phys. Rev. A 13, 1067 (1976).

[23]W. G. Harter and C. W. Patterson, *A Unitary Calculus for Electronic Orbitals*, Lecture Notes in Physics No. 49 (Springer-Verlag, New York, 1976).

[24]C. W. Patterson and W. G. Harter, Phys. Rev. A 15, 2372 (1977).

[25]I. M. Gelfand and M. Zetlin, Dokl. Akad. Nauk SSSR 71, 825 (1950).

[26]L. C. Biedenharn, A. Giovannini and J. D. Louck, J. Math. Phys. 8, 691 (1967).

[27]J. D. Louck, Am. J. Phys. 38, 3 (1970).

[28]H. W. Galbraith, J. Chem. Phys. 68, 1677 (1978).

[29]G. R. Guther-Mohr, C. H. Townes, and J. H. Van Vleck, Phys. Rev. 94, 1191 (1954).

[30](a) P. N. Yi, I. Ozier, and C. H. Anderson, Phys. Rev. 165, 92 (1968); (b) P. N. Yi, I. Ozier, and N. F. Ramsey, J. Chem. Phys. 55, 5215 (1971).

[31]M. D. Levenson and A. L. Schawlow, Phys. Rev. A 6, 10 (1972).

[32]M. Quack, Mol. Phys. 34, 447 (1977).

[33]J. D. Louck and H. W. Galbraith, Rev. Mod. Phys. 48, 69 (1976).

[34]C. W. Patterson and W. G. Harter, J. Math. Phys. 17, 1125 (1976); and 17, 1137 (1976).

[35]G. de B. Robinson, *Representations of the Symmetric Group* (Toronto University, Toronto, 1960).

[36]K. R. Lea, M. J. M. Leask, and W. P. Wolf, J. Phys. Chem. Solids 23, 138 (1962); W. G. Harter and C. W. Patterson, J. Math. Phys. (to be published).

[37]A. J. Coleman, *Queen's Paper in Pure and Applied Mathematics*, No. 4 (Queen's University, Kingston, Ontario, 1966), p. 17.